Available online at www.sciencedirect.com
SCIENCE DIRECT®
Journal of Computational Physics 192 (2003) 124–156
JOURNAL OF COMPUTATIONAL PHYSICS
www.elsevier.com/locate/jcp

A weak Legendre collocation spectral method for the solution of the incompressible Navier–Stokes equations in unstructured quadrilateral subdomains

Dimitris Kondaxakis *, Sokrates Tsangaris

Fluids Section, School of Mechanical Engineering, National Technical University of Athens, 9 Heroon Polytechniou Avenue, 15773 Zografou, Athens, Greece

Received 17 February 2003; received in revised form 1 July 2003; accepted 2 July 2003

Abstract

A weak Legendre spectral method is developed for the solution of the primitive variable formulation of the unsteady incompressible Navier–Stokes equations, in general two-dimensional and axisymmetric geometries. A semi-implicit projection method is utilized for the temporal approximation and for decoupling the velocity field from the pressure field. A series of elliptic boundary value problems arises from the above procedure, each of which is spatially discretized by a weak collocation method in multiple nonoverlapping subdomains. In particular, a modified variational formulation of the partial differential equations is presented which leads, after discretization, to a weak multidomain approximation of the corresponding problems. A weak formalism for the influence matrix technique is also developed, which is consistent with the spatial discretization scheme and successfully separate the equations for the internal nodes from the ones governing the interface unknowns. A method of dealing with the singularity problem faced by the weak formulation at axisymmetric problems is proposed, while a combination of direct methods is studied for tackling effectively the linear algebraic systems resulting from the full discretization. Exponential convergence is demonstrated for a plethora of Stokes and Navier–Stokes simulations.

Keywords: Weak collocation Legendre method; Domain decomposition; Influence matrix; Axisymmetric simulation

1. Introduction

Spectral methods form an efficient and highly accurate family of techniques for solving differential and integral equations [1,2]. Their utilization in computational fluid dynamics has proven to be very profitable, particularly when accuracy plays a fundamental role [3–6]. Domain decomposition algorithms, on the other hand, have helped spectral methods to overcome some of their inherent limitations, extending their applicability in complex geometries and allowing them to exploit modern parallel computer architectures.

* Corresponding author.
E-mail address: kond@fluid.mech.ntua.gr (D. Kondaxakis).

0021-9991/$ - see front matter © 2003 Elsevier B.V. All rights reserved.
doi:10.1016/S0021-9991(03)00350-4

Spectral domain decomposition methods have successfully found their way through the fields of both incompressible [7,8], as well as compressible [9–11] flow simulations.

In the present paper, we present a combination of a nonoverlapping Legendre spectral collocation domain decomposition method, with a semi-implicit projection scheme in order to compute steady and unsteady solutions of the incompressible Navier–Stokes equations in general two-dimensional and axisymmetric domains. The temporal discretization method belongs to the class of time-splitting algorithms [12–18] used to decouple the velocity from the pressure calculations. As for the spatial discretization of the elliptic scalar problems that stem from the application of the above scheme, we utilize a modified variational formulation, which leads to a discrete weak Legendre collocation approximation in multiple subdomains. This technique has been used before, in [19], to treat simple elliptic equations in rectangularly decomposable domains and in [9] to deal with the interface conditions for the viscous terms at compressible simulations. It can be viewed as a special form of the so-called penalty method used for incompressible simulations in [20] and is similar but different from the spectral flux balance interface technique [21–23]. An analysis of the Chebyshev approximation is considered in [24]. We use this method both for imposing Neumann boundary conditions with enhanced accuracy and for treating naturally the equations that govern the interface unknowns. We also provide a unified form of the method, which is able to handle effectively unstructured subdomain decompositions by treating successfully nodes that belong simultaneously to the Neumann portion of the boundary and to two or more subdomains. We apply this method to the solution of the incompressible flow equations and find that it overcomes many of the difficulties faced by the strong collocation approximation when applied to mixed Dirichlet–Neumann boundary value problems in generally decomposed curvilinear topologies. We also furnish a weak formulation of the widely used influence matrix technique (see [25,26]), so as to combine it successfully with the spatial discretization method in order to perform a decoupling of the equations for the internal nodes from those that govern the interface and some of the boundary unknowns.

When the above methods are applied to axisymmetric problems, they encounter a singularity on the axis of symmetry, despite the fact that boundary conditions have to be imposed in order to close the system of discrete equations. A similar problem has been dealt before in [27] by transforming the dependent variables of the flow field. With such a method, the calculation of the primitive variables on the axis of symmetry becomes very difficult (if not impossible) in generally decomposed domain configurations, since the transformation performed is not invertible at the axis. We propose a method which is very well suited to the overall scheme used and accomplishes to eliminate the pole singularity that appears in the differential equations and boundary conditions, while allowing the usage of general domain decompositions and exhibiting spectrally converged results.

Finally, in an attempt to increase the efficiency of direct methods in multiple domain algorithms, we study the collaboration of the LU-factorization method with the matrix-diagonalization one, in the framework of complete Navier–Stokes simulations. The method proposed here has many differences from other well-established domain decomposition methods (like the spectral element method) basically in the context of the spatial discretization and which will become clear after the subsequent presentation.

This paper is organized as follows. Section 2 gives the basic primitive variable form of the incompressible Navier–Stokes equations. In Section 3, the temporal discretization scheme is briefly reviewed. The spatial approximation method for model elliptic problems as well as some aspects of its implementation to the full system of the flow equations are presented in Section 4. Finally, Section 5 is devoted to the study of various simulation results, beginning from simple problems and ending with complicated incompressible flow solutions.

2. Incompressible Navier–Stokes equations

We consider a two-dimensional open and bounded domain $\Omega \subset \Re^2$ with a Lipschitz continuous boundary $\partial\Omega$, and a time interval $I = (0, T] \subset \Re$. The Navier–Stokes equations that govern the motion of an incompressible fluid with constant viscosity in nondimensional form read:

$$\begin{aligned} &D[\vec{u}] = 0, \\ &\frac{\partial \vec{u}}{\partial t} + \vec{N}[\vec{u}] = -\vec{G}[p] + \frac{1}{Re}\vec{L}[\vec{u}] + \vec{f} \end{aligned} \tag{1}$$

in Ω, for all $t \in I$. In these equations, the dimensional variables of space ($\vec{x}'$), time (t'), velocity ($\vec{u}'$), pressure (p'), and body force per unit volume ($\vec{f}'$) have been scaled by:

$$\vec{x} = \vec{x}'/l_{\mathrm{r}},$$

$$t = t'/(l_{\mathrm{r}}/\|\vec{u}_{\mathrm{r}}\|),$$

$$\vec{u} = \vec{u}'/\|\vec{u}_{\mathrm{r}}\|,$$

$$p = p'/(\rho\|\vec{u}_{\mathrm{r}}\|^2),$$

$$\vec{f} = \vec{f}'/(\rho\|\vec{u}_{\mathrm{r}}\|^2/l_{\mathrm{r}}),$$

where $\|\vec{u}_{\mathrm{r}}\|$ is a reference velocity magnitude, l_{r} is a reference length scale and ρ is the constant density. The Reynolds number is defined as $Re = \|\vec{u}_{\mathrm{r}}\| l_{\mathrm{r}} \rho/\mu$, where μ is the fluid viscosity. It is clear that the pressure variable in the incompressible Navier–Stokes equations acts as a Lagrange multiplier that ensures the solenoidity of the velocity vector field. In order to define the form of the differential operators that appear in the Navier–Stokes equations, we need to distinguish between two-dimensional flows and axisymmetric ones. For two-dimensional flows we use a Cartesian frame of reference and denote the spatial coordinates as (x, y). On the other hand, when we deal with an axisymmetric problem, we use a cylindrical frame of reference where x is the axial coordinate and y is the radial one. Accordingly, u is the axial and v the radial velocity components. By using this notation, we have:

$$D[\vec{u}] = \frac{\partial u}{\partial x} + \frac{\partial v}{\partial y} + a\frac{v}{y},$$

$$\vec{N}[\vec{u}] = \begin{pmatrix} u\frac{\partial u}{\partial x} + v\frac{\partial u}{\partial y} \\ u\frac{\partial v}{\partial x} + v\frac{\partial v}{\partial y} \end{pmatrix},$$

$$\vec{G}[p] = \begin{pmatrix} \frac{\partial p}{\partial x} \\ \frac{\partial p}{\partial y} \end{pmatrix},$$

$$\vec{L}[\vec{u}] = \begin{pmatrix} \frac{\partial^2 u}{\partial x^2} + \frac{\partial^2 u}{\partial y^2} + a\frac{1}{y}\frac{\partial u}{\partial y} \\ \frac{\partial^2 v}{\partial x^2} + \frac{\partial^2 v}{\partial y^2} + a\left(\frac{1}{y}\frac{\partial v}{\partial y} - \frac{v}{y^2}\right) \end{pmatrix},$$

where $a = 0, 1$ for two-dimensional and axisymmetric flows, respectively.

The set of equations (1) must be equipped with proper boundary and initial conditions. The boundary $\partial\Omega$ can be decomposed into two open, bounded and mutually disjoint sets namely Γ^u_{D} and Γ^u_{N} such that $\bar{\Gamma}^u_{\mathrm{D}} \cup \bar{\Gamma}^u_{\mathrm{N}} = \partial\Omega$, $\Gamma^u_{\mathrm{D}} \cap \Gamma^u_{\mathrm{N}} = 0$, on which the boundary conditions for the u-component of the velocity vector are imposed. In a similar way, we define two sets Γ^v_{D} and Γ^v_{N} for the boundary conditions of the v-velocity

component. Four scalar fields are set as $g_u : \Gamma_{\mathrm{D}}^u \times I \to \Re$, $g_v : \Gamma_{\mathrm{D}}^v \times I \to \Re$, $h_u : \Gamma_{\mathrm{N}}^u \times I \to \Re$ and $h_v : \Gamma_{\mathrm{N}}^v \times I \to \Re$. The boundary conditions that must be specified on $\partial\Omega$ are:

$$\begin{aligned} u &= g_u \text{ on } \Gamma_{\mathrm{D}}^u, \quad t \in I, \\ v &= g_v \text{ on } \Gamma_{\mathrm{D}}^v, \quad t \in I, \end{aligned} \tag{2a}$$

$$\begin{aligned} \frac{\partial u}{\partial n} &= \nabla u \cdot \vec{n} = h_u \text{ on } \Gamma_{\mathrm{N}}^u, \quad t \in I, \\ \frac{\partial v}{\partial n} &= \nabla v \cdot \vec{n} = h_v \text{ on } \Gamma_{\mathrm{N}}^v, \quad t \in I. \end{aligned} \tag{2b}$$

The boundary conditions (2a) are of Dirichlet type and must satisfy the compatibility condition that $\int_{\partial\Omega} \vec{g} \cdot \vec{n} = 0$ if $\bar{\Gamma}_{\mathrm{D}}^u = \bar{\Gamma}_{\mathrm{D}}^v = \partial\Omega \ \forall t \in I$, with $\vec{g} = (g_u, g_v)$, while the boundary conditions (2b) are of Neumann type with $\vec{n}$ the outward unit normal vector on $\partial\Omega$. We must say that here and in some parts of the following text, we indicate neither the integration measure $\mathrm{d}\vec{x}$ in the double integrals nor $\mathrm{d}\sigma$ in the line integrals, for the sake of simplicity. The initial condition that must be specified for the velocity field is:

$$\vec{u} = \vec{u}_0 \quad \text{in } \Omega, \text{ for } t = 0,$$

with $\vec{u}_0 : \Omega \to \Re^2$. The choice of the initial velocity field is not arbitrary. It must certainly be divergence-free, so that the continuous problem has a classical solution. A more rigorous discussion on the set of compatibility conditions that the initial condition must satisfy is supplied in [28]. Notice that no boundary or initial conditions are required for the pressure.

Let us define, at this point, some functional spaces that will prove to be very helpful in the subsequent discussion. We shall indicate with $[L^p(\Omega)]^2$ $(1 \leqslant p \leqslant \infty)$, the space of vector functions $F : \Omega \to \Re^2$ whose components belong to $L^p(\Omega)$, and with $[H^m(\Omega)]^2$ $(m = 0, 1, 2, \ldots)$, the space of vector functions whose components belong to the Sobolev space of mth order $H^m(\Omega)$. If we derive the weak form of Eq. (1) considering the boundary and initial conditions, it is clear that we have the velocity field belonging to the space:

$$Q_v = \{\vec{u} \in [H^1(\Omega)]^2 \,|\, u = g_u \text{ on } \Gamma_{\mathrm{D}}^u \text{ and } v = g_v \text{ on } \Gamma_{\mathrm{D}}^v\},$$

and the pressure to the space:

$$Q_p = \left\{ p \in L^2(\Omega) \,\middle|\, \int_\Omega p = 0 \text{ if } \bar{\Gamma}_{\mathrm{D}}^u = \bar{\Gamma}_{\mathrm{D}}^v = \partial\Omega \right\},$$

while $\vec{f}$ belongs to the dual space of Q_v for all times.

3. Temporal approximation method

In this section we use the method of lines in order to discretize the temporal differential operators while leaving the spatial ones continuous and so formulating a semi-discrete version of the Navier–Stokes equations. We utilize the projection method which was originally proposed by Hugues and Randriamampianina [16], and was implemented in the framework of the strong Chebyshev spectral collocation approximation. This projection method is second order accurate in both velocity and pressure and is based on a combination of Adams–Bashforth and backward differentiation formula schemes. The fractional steps proceed as follows (the superscripts denote the discrete time levels):

- Pressure predictor step:
  Solve at each time step, the elliptic equation:

$$D[\vec{G}[\bar{p}^{n+1}]] = D[-2\vec{N}^n + \vec{N}^{n-1} + \vec{f}^{n+1}]$$

  in Ω, with:

$$\frac{\partial \bar{p}^{n+1}}{\partial n} = \vec{n} \cdot \left\{ \frac{-3\vec{g}^{n+1} + 4\vec{u}^n - \vec{u}^{n-1}}{2\Delta t} - 2\vec{N}^n + \vec{N}^{n-1} + \frac{1}{Re}\left(2\vec{R}^n - \vec{R}^{n-1}\right) + \vec{f}^{n+1} \right\}$$

  on $\Gamma^u_{\mathrm{D}} \cap \Gamma^v_{\mathrm{D}}$ and appropriate Dirichlet or Neumann boundary conditions imposed on $\partial\Omega \setminus (\Gamma^u_{\mathrm{D}} \cap \Gamma^v_{\mathrm{D}})$. The diffusion operator R is defined as:

$$\vec{R}[\vec{u}] = \vec{G}[D[\vec{u}]] - \vec{L}[\vec{u}]$$

  and has this form, in order to improve the stability of the solution (see also [12,13,15]).
- Velocity predictor step:
  Next solve the following equation:

$$\vec{L}[\vec{u}^*] - \frac{3Re}{2\Delta t}\vec{u}^* = Re\left\{ \frac{-4\vec{u}^n + \vec{u}^{n-1}}{2\Delta t} + 2\vec{N}^n - \vec{N}^{n-1} + \vec{G}[\bar{p}^{n+1}] - \vec{f}^{n+1} \right\}$$

  in Ω, with:

$$u^* = g_u^{n+1} \quad \text{on } \Gamma^u_{\mathrm{D}},$$

$$v^* = g_v^{n+1} \quad \text{on } \Gamma^v_{\mathrm{D}},$$

$$\frac{\partial u^*}{\partial n} = h_u^{n+1} \quad \text{on } \Gamma^u_{\mathrm{N}},$$

$$\frac{\partial v^*}{\partial n} = h_v^{n+1} \quad \text{on } \Gamma^v_{\mathrm{N}}.$$

- Correction step:
  Finally, solve the elliptic equation:

$$D[\vec{G}[\tilde{p}^{n+1}]] = D[\vec{u}^*]$$

  in Ω, with:

$$\frac{\partial \tilde{p}^{n+1}}{\partial n} = 0 \quad \text{on } \Gamma^u_{\mathrm{D}} \cap \Gamma^v_{\mathrm{D}},$$

  and problem-dependent Dirichlet or Neumann boundary conditions on $\partial\Omega \setminus (\Gamma^u_{\mathrm{D}} \cap \Gamma^v_{\mathrm{D}})$. Then compute the corrected pressure and velocity fields:

$$p^{n+1} = \bar{p}^{n+1} + \frac{3}{2\Delta t}\tilde{p}^{n+1},$$

$$\vec{u}^{n+1} = \vec{u}^* - \vec{G}[\tilde{p}^{n+1}]$$

  in $\bar{\Omega} = \Omega \cup \partial\Omega$.

For the initial step we have used a consistent first-order method to start the scheme.

This projection method is very efficient and possesses a good temporal behavior for sufficiently large time integration. In the subsequent sections concerning the spatial approximation, we use polynomials of the same degree for both the velocity components as well as for the pressure, in order to facilitate the multi-domain implementation of the algorithm. The above-mentioned time-splitting scheme uses the normal momentum equation at the boundary to close the discrete system, rather than the incompressibility equation. With this technique, there is no need of satisfying any form of compatibility condition between the function spaces that the velocity and pressure fields belong to (like the inf–sup condition), since there are no spurious pressure modes present in the solution. At the end of the correction step the final velocity field is divergence-free at all the inner collocation points, but the boundary condition on the tangential velocity component is not exactly satisfied. The error term (slip velocity) is numerically checked to be $O(\Delta t^3)$ and, as a consequence, its effect on the overall accuracy of the method is negligible. This time discretization procedure decomposes the solution of the Navier–Stokes equations into a cascade of elliptic kernels (namely Helmholtz and Poisson equations for the two-dimensional case). In the following section, we demonstrate an efficient way of solving these problems in the framework of a weak spectral multidomain collocation discretization.

4. Spatial approximation method

In the following sections, we deal with both the continuous and discrete versions of the spatial approximation method applied to a generic form of a linear elliptic boundary value problem. Subsequently, we report some of the algorithmic aspects which can be used in order to make the scheme computationally efficient and finally we comment on the implementation of the method to the semi-discretized form of the Navier–Stokes equations.

4.1. Continuous formulation

In this section, we focus on the spatial approximation of general elliptic partial differential equations of second order in a two-dimensional space. Let us define a linear operator of the form:

$$L[u] = -\sum_{i=1}^{2}\sum_{j=1}^{2}\frac{\partial}{\partial x_i}\left(a_{ij}\frac{\partial u}{\partial x_j}\right) + \sum_{j=1}^{2} a_j\frac{\partial u}{\partial x_j} + a_0 u,$$

where we have used the notation that $\vec{x} = (x_1, x_2) = (x, y)$ is a point in $\Re^2$. We assume that the coefficients a_{ij}, a_j, a_0 are functions of the spatial-independent variables and belong to $L^\infty(\Omega)$. The above operator is said to be elliptic in Ω, if for every $\vec{x} \in \Omega$ the following relation holds:

$$\sum_{i=1}^{2}\sum_{j=1}^{2} a_{ij}(\vec{x})\xi_i\xi_j \neq 0 \quad \text{for every } \vec{\xi} \neq \vec{0}$$

and strongly elliptic, if there exists a constant $\mu > 0$, such that:

$$\sum_{i=1}^{2}\sum_{j=1}^{2} a_{ij}(\vec{x})\xi_i\xi_j \geqslant \mu\left\|\vec{\xi}\right\| \quad \text{for every } \vec{\xi} \in \Re^2 \text{ and every } \vec{x} \in \Omega.$$

Suppose that we have the following elliptic boundary value problem:

$$\begin{cases} L[u] = f & \text{in } \Omega, \\ u = g & \text{on } \Gamma_{\mathrm{D}}, \\ \frac{\partial u}{\partial n_L} = h & \text{on } \Gamma_{\mathrm{N}}, \end{cases} \tag{3}$$

with: $\partial u/\partial n_L = \vec{D}_L[u] \cdot \vec{n} = \sum_{i=1}^{2} \sum_{j=1}^{2} a_{ij}(\partial u/\partial x_j) n_i$, and $\Gamma_D \cap \Gamma_N = 0, \bar{\Gamma}_D \cup \bar{\Gamma}_N = \partial\Omega$. The above problem is a general form of the elliptic kernels which the Navier–Stokes equations are decomposed into, by the time discretization method. The variational formulation of this problem reads:

$$\begin{cases} u \in U = \{u \in H^1(\Omega) \,|\, u = g \text{ on } \Gamma_D\}, \\ a(u,v) = b(v) \ \forall v \in V = \{v \in H^1(\Omega) \,|\, v = 0 \text{ on } \Gamma_D\}, \end{cases} \tag{4}$$

where the above bilinear and linear forms are given as:

$$a(u,v) = \int_\Omega \int \left(\sum_{i=1}^{2} \sum_{j=1}^{2} a_{ij} \frac{\partial u}{\partial x_j} \frac{\partial v}{\partial x_i} + \sum_{j=1}^{2} a_j \frac{\partial u}{\partial x_j} v + a_0 uv \right),$$

$$b(v) = \int_\Omega \int fv + \int_{\Gamma_N} hv.$$

We have silently assumed that the functions f, h belong to $L^2(\Omega)$. The classical solution of the boundary value problem (3) is proven to be also a weak solution to the variational formulation (4).

Next, we subdivide the computational domain Ω, into quadrilateral nonoverlapping subdomains Ω^m, $m \in M$ (M being a set of positive integers) each of which is open and bounded, in a structured or generally unstructured way so as $\bar{\Omega} = \bigcup_{m \in M} \bar{\Omega}^m$, and $\Omega^k \cap \Omega^l = 0$ for $k \neq l$. The assumptions we make on this subdivision are that we allow the closures of two neighboring subdomains to intersect only at a point or along an entire side, and that the subdomain boundaries do not move in time. We also define $\Gamma_N^m = \partial\Omega^m \cap \Gamma_N$. After all of these, the functionals that appear in the variational formulation take the following form:

$$a(u,v) = \sum_{m \in M} \left\{ \int_{\Omega^m} \int \left(\sum_{i=1}^{2} \sum_{j=1}^{2} a_{ij}^m \frac{\partial u^m}{\partial x_j} \frac{\partial v^m}{\partial x_i} + \sum_{j=1}^{2} a_j^m \frac{\partial u^m}{\partial x_j} v^m + a_0^m u^m v^m \right) \right\},$$

$$b(v) = \sum_{m \in M} \left\{ \int_{\Omega^m} \int f^m v^m + \int_{\Gamma_N^m} h^m v^m \right\},$$

where we have indicated by z^m the restriction of the function z to the subdomain Ω^m.

In view of describing the discrete formulation of the boundary value problem, we shall alter the above variational form first by making a few more stringent assumptions on the regularity of the function u. To this end, we assume that:

$$u \in \hat{U} = \{u \in H^2(\Omega) \,|\, u = g \text{ on } \Gamma_D\},$$

and we see that the bilinear form a is equivalent to:

$$a(u,v) = \sum_{m \in M} \left\{ \int_{\Omega^m} \int L^m[u^m] v^m + \oint_{\partial\Omega^m} \left(\vec{D}_L^m[u^m] \cdot \vec{n}^m \right) v^m \right\}.$$

By the superscript m on the differential operators, we indicate not only the restriction of their action on the subspace of functions defined on Ω^m, but also the replacement of the coefficient functions by their restrictions in the specific subdomain. It is obvious that with the above form we only require:

$$v \in \hat{V} = \{v \in L^2(\Omega) \,|\, v = 0 \text{ on } \Gamma_D\}.$$

We assume that there exists a family of isomorphisms (continuous and invertible operators) $\vec{F}^m,\ m \in M$, that map each of the quadrilateral subdomains $\bar{\Omega}^m$ onto the reference square (or parent element) $\bar{D} = [-1,1]^2$, in such a way that the subdomain border $\partial\Omega^m$ is also mapped on the reference one ∂D. We denote any point in $\bar{D}$ by the ordered pair of real numbers $\vec{r} = (r_1, r_2) = (r, s)$ and any point in $\bar{\Omega}^m$ by $\vec{x}^m = (x^m, y^m)$. By usage of the above notation, we can write:

$$\vec{F}^m : \bar{D} \to \bar{\Omega}^m,\ \ \vec{F}^m \in [C^2(\bar{D})]^2 : \vec{x}^m = \vec{F}^m(\vec{r}), \quad m \in M.$$

The operators $\vec{F}^m$ are vector-valued functions which are initially unknown, but we postpone their description until the discussion about the discrete system of equations. At this point, we have for each subdomain the scalar functions:

$$x^m = x^m(r,s),$$

$$y^m = y^m(r,s)$$

for $|r|, |s| \leqslant 1, m \in M$. The transformation Jacobian is defined by the formula:

$$J^m = \frac{\partial x^m}{\partial r}\frac{\partial y^m}{\partial s} - \frac{\partial x^m}{\partial s}\frac{\partial y^m}{\partial r},$$

for $m \in M$ and is different from zero for every point in each subdomain. Moreover, the Jacobian never changes sign inside a subdomain and if $J^m > 0$ then the boundary $\partial\Omega^m$ is positively oriented.

We now discuss the calculation of the double and line integrals that appear in the linear forms of the variational formulation, under the above-mentioned coordinate transformation. For a function $q^m \in L^2(\Omega^m)$, we have:

$$\int_{\Omega^m}\int q^m = \int_{s=-1}^{1}\int_{r=-1}^{1} q^m(x^m(r,s), y^m(r,s))|J^m(r,s)|\,\mathrm{d}r\,\mathrm{d}s.$$

Let us define the four sides of the subdomain $\bar{\Omega}^m$ as $\Gamma^{m,p},\ p = 1,\ldots,4$, so that $\bigcup_{p=1}^4 \bar{\Gamma}^{m,p} = \partial\Omega^m$. In the same manner, we define the four sides of the parent element $\bar{D}$ as $S^p,\ p = 1,\ldots,4$, with $\bigcup_{p=1}^4 \bar{S}^p = \partial D$. Specifically, we set:

$$S^1 = \{\vec{r} = (r,s) \in \partial D \,|\, s = -1,\ |r| < 1\},$$

$$S^2 = \{\vec{r} = (r,s) \in \partial D \,|\, r = 1,\ |s| < 1\},$$

$$S^3 = \{\vec{r} = (r,s) \in \partial D \,|\, s = 1,\ |r| < 1\},$$

$$S^4 = \{\vec{r} = (r,s) \in \partial D \,|\, r = -1,\ |s| < 1\}.$$

As we have already mentioned, the coordinate transformation operator maps each of the $\Gamma^{m,p}$ onto each of the S^p, so that we can symbolically write $\Gamma^{m,p} = \vec{F}^m(S^p), m \in M,\ p = 1,\ldots,4$. Suppose that we have a vector-valued function $\vec{Q}^m \in [L^2(\partial\Omega^m)]^2$, then the formula for the evaluation of the line integral is:

$$\oint_{\partial\Omega^m} \vec{Q}^m \cdot \vec{n}^m = \sum_{p=1}^{4}\left\{\int_{\sigma=\bar{S}^p{}^{-1}}^{1} \vec{Q}^m(x^m(r,s), y^m(r,s)) \cdot \vec{N}^{m,p}\ \mathrm{d}\sigma^p\right\},$$

where:

$$\mathrm{d}\sigma^p = \begin{cases} \mathrm{d}r & \text{on } S^1,\ S^3, \\ \mathrm{d}s & \text{on } S^2,\ S^4, \end{cases}$$

$$\vec{N}^{m,p} = O_1^p O_2^m \vec{N}_0^{m,p},$$

$$O_1^p = \begin{cases} 1 & \text{on } S^1,\ S^2, \\ -1 & \text{on } S^3,\ S^4, \end{cases}$$

$$O_2^m = \operatorname{sign}(J^m),$$

$$\vec{N}_0^{m,p} = \begin{cases} \left(\frac{\partial y^m}{\partial r}, -\frac{\partial x^m}{\partial r}\right) & \text{on } S^1,\ S^3, \\ \left(\frac{\partial y^m}{\partial s}, -\frac{\partial x^m}{\partial s}\right) & \text{on } S^2,\ S^4. \end{cases}$$

Exactly in the same way, if we are given the function $q^m = \vec{Q}^m \cdot \vec{n}^m \in L^2(\partial\Omega^m)$, then the line integral takes the form:

$$\oint_{\partial\Omega^m} q^m = \sum_{p=1}^{4} \left\{ \int_{\substack{\sigma=-1 \\ S^p}}^{1} q^m(x^m(r,s), y^m(r,s)) \left\| \vec{N}^{m,p} \right\| \mathrm{d}\sigma^p \right\}.$$

After all of these, the modified variational formulation of the generalized boundary value problem (3), is:

$$\begin{cases} u \in \hat{U}, \\ a(u,v) = b(v) \quad \forall v \in \hat{V}, \end{cases} \tag{5}$$

where:

$$a(u,v) = \sum_{m\in M} \left\{ \begin{array}{c} \int_{s=-1}^{1} \int_{r=-1}^{1} L^m[u^m(x^m(r,s), y^m(r,s))] v^m(x^m(r,s), y^m(r,s)) |J^m(r,s)| \mathrm{d}r\,\mathrm{d}s \\ + \sum_{p=1}^{4} \left(\int_{\substack{\sigma=-1 \\ S^p}}^{1} \left(\vec{D}_L^m[u^m(x^m(r,s), y^m(r,s))] \cdot \vec{N}^{m,p} \right) v^m(x^m(r,s), y^m(r,s)) \mathrm{d}\sigma^p \right) \end{array} \right\}$$

$$b(v) = \sum_{m\in M} \left\{ \begin{array}{c} \int_{s=-1}^{1} \int_{r=-1}^{1} f^m(x^m(r,s), y^m(r,s)) v^m(x^m(r,s), y^m(r,s)) |J^m(r,s)| \mathrm{d}r\,\mathrm{d}s \\ + \sum_{p\in P^m} \left(\int_{\substack{\sigma=-1 \\ S^p}}^{1} h^m(x^m(r,s), y^m(r,s)) v^m(x^m(r,s), y^m(r,s)) \left\| \vec{N}^{m,p} \right\| \mathrm{d}\sigma^p \right) \end{array} \right\}$$

and P^m being the index set defined as:

$$P^m = \left\{ p \,|\, 1 \leqslant p \leqslant 4,\ \Gamma^{m,p} \subseteq \Gamma_{\mathrm{N}}^m,\ \Gamma^{m,p} = \vec{F}^m(S^p), m \in M \right\}.$$

4.2. Discrete formulation

In this section, we proceed by deriving the discrete version of the modified variational formulation of the generalized boundary value problem. Given a positive integer N, we define the space $P_N(\bar{D})$, to be the space

of continuous functions up to the boundary $f : \bar{D} \to \Re$, such that f is an algebraic polynomial of degree less or equal than N in each independent spatial variable. The approximants u_N^m of the restrictions u^m of u, in each subdomain, belong to $P_N(\bar{D})$.

In order to define the spectral collocation method, we need to introduce a set of distinct points (pseudospectral grid), that covers the closed parent element $\bar{D}$. We consider the integer vector index $\vec{j} = (j_1, j_2), 0 \leqslant j_1, j_2 \leqslant N$ and define the set:

$$J = \left\{ \vec{j} = (j_1, j_2), 0 \leqslant j_1, j_2 \leqslant N \,|\, \vec{r}_{\vec{j}} = (r_{j_1}, s_{j_2}) \in \bar{D} \right\}.$$

By using this set, we can express the collocation grid on $\bar{D}$ as the set of nodes $\vec{r}_{\vec{j}}, \vec{j} \in J$. In a similar manner, we define the boundary index sets to be:

$$J_b^p = \left\{ \vec{j} = (j_1, j_2), 0 \leqslant j_1, j_2 \leqslant N \,|\, \vec{r}_{\vec{j}} = (r_{j_1}, s_{j_2}) \in \bar{S}^p \right\}, \quad p = 1, \ldots, 4.$$

After the application of the coordinate transformation operators $\vec{F}^m$, $m \in M$ we can calculate the grids $\vec{x}_{\vec{j}}^m = (x_{j_1}^m, y_{j_2}^m) = \vec{F}^m(\vec{r}_{\vec{j}}) \in \bar{\Omega}^m$, $\vec{j} \in J$, that cover each subdomain. Next, we introduce a global numbering of nodes by assigning a different scalar index to each node and define the set:

$$J^{\mathrm{G}} = \{ l \,|\, \vec{x}_l = (x_l, y_l) \in \bar{\Omega} \},$$

where l is a positive integer. The dimension of this set is equal to the total number of the grid points. By using such a notation, we are able to write the whole mesh as $\vec{x}_l, l \in J^{\mathrm{G}}$. Similarly, we can denote the subsets of the indices of the nodes, in the global numbering system, on which we impose Dirichlet or Neumann boundary conditions as $J_{b,\mathrm{D}}^{\mathrm{G}} \subset J^{\mathrm{G}}$ and $J_{b,\mathrm{N}}^{\mathrm{G}} \subset J^{\mathrm{G}}$, respectively.

It is now necessary to define an operator $G : M \times J \to J^{\mathrm{G}}$ which determines the correlations between the subdomains, the local and the global indices. Given the index of a specific subdomain (say m) and the local index of a node which belongs to this subdomain (say $\vec{j}$), we get after the application of the above operator, the index $l = G(m, \vec{j})$, of the specific node in the global numbering system. By this, we mean that:

$$\vec{x}_l = \vec{x}_{\vec{j}}^m = \vec{F}^m(\vec{r}_{\vec{j}}), \quad m \in M, \ \vec{j} \in J, \ l \in J^{\mathrm{G}}.$$

It is obvious that since a given node may belong to more than one subdomains, the operator G is not invertible.

A tensor-product Lagrange basis of $P_N(\bar{D})$ is defined by the relations:

$$\phi^{\vec{j}}(\vec{r}) : \bar{D} \to \Re, \quad \vec{j} \in J,$$

$$\phi^{\vec{j}}(\vec{r}) = C^{j_1}(r) C^{j_2}(s) \in P_N(\bar{D}),$$

$$C^{j_1}(r), C^{j_2}(s) : [-1, 1] \to \Re,$$

$$C^b(t_a) = \delta_a^b = \begin{cases} 0, & a \neq b, \\ 1, & a = b, \end{cases} \quad t_a \in [-1, 1], \ 0 \leqslant a, b \leqslant N,$$

$$\phi^{\vec{j}}(\vec{r}_{\vec{i}}) = \delta_{\vec{i}}^{\vec{j}} = \begin{cases} 0, & \vec{i} \neq \vec{j}, \\ 1, & \vec{i} = \vec{j}, \end{cases} \quad \vec{i}, \vec{j} \in J.$$

In this way, we are able to express the approximants u_N^m as:

$$u_N^m(\vec{r}) = \sum_{\vec{j}\in J} \langle u_N^m \rangle_{\vec{j}} \phi^{\vec{j}}(\vec{r}),$$

where: $\langle u_N^m \rangle_{\vec{j}} = u_N^m(\vec{r}_{\vec{j}}) = u_N^m(r_{j_1}, s_{j_2})$.

The coordinate transformation operators are actually calculated by the isoparametric technique (see [2,4,7,10]), meaning that the geometric variables are defined by the same interpolation rules as the unknown function of the differential equation, namely:

$$\vec{x}_N^m \in [P_N(\bar{D})]^2 : \vec{x}_N^m(\vec{r}) = \vec{F}_N^m(\vec{r}) = \sum_{\vec{j}\in J} \left\langle \vec{x}_N^m \right\rangle_{\vec{j}} \phi^{\vec{j}}(\vec{r}).$$

First, the physical mesh is specified on the subdomain boundaries: $\vec{x}_N^m(\vec{r}_{\vec{j}})$, $j \in J_b^p$, $p = 1, \ldots, 4, m \in M$, then by using interpolation with bilinear blending functions, the remaining internal grid points are calculated. The Jacobian and metric factors needed in the differential and integral expressions are calculated pseudospectrally, meaning that all the approximate derivatives are computed by differentiating the interpolants at the collocation nodes. It is now the appropriate time to say that the discrete spatial approximation must be conforming so that the grid lines coincide along subdomain boundaries. Actually, we can also have different polynomial orders in each independent spatial variable and in each subdomain as long as the approximation remains conforming, but then the whole presentation would become extremely complicated.

Next, we fix a family of weights $w_j > 0, 0 \leqslant j \leqslant N$, and set the bilinear form:

$$(f, g)_N = \sum_{\vec{j}\in J} \langle f \rangle_{\vec{j}} \langle g \rangle_{\vec{j}} \omega_{\vec{j}},$$

where: $\langle f \rangle_{\vec{j}} = f(r_{j_1}, s_{j_2}), \langle g \rangle_{\vec{j}} = g(r_{j_1}, s_{j_2})$, and $\omega_{\vec{j}} = w_{j_1} w_{j_2}$. By the existence of the above-mentioned Lagrange basis, this form is ensured to be a discrete inner product on $P_N(\bar{D})$. If we specify the $\vec{r}_{\vec{j}}$ and $\omega_{\vec{j}}$, $\vec{j} \in J$, to be the knots and weights, respectively, of quadrature formulas of Gaussian type, then we can approximate the double integral $\int_{s=-1}^{1} \int_{r=-1}^{1} fg \, \mathrm{d}r \, \mathrm{d}s$ by $(f, g)_N$, with maximum precision. Under the same reasoning, we may write:

$$\int_{\sigma=-1}^{1} f \, \mathrm{d}\sigma^p = \sum_{\vec{j}\in J_b^p} \langle f \rangle_{\vec{j}} \omega_{\vec{j}}^p,$$

where:

$$\omega_{\vec{j}}^p = \begin{cases} w_{j_1}, & p = 1, 3, \\ w_{j_2}, & p = 2, 4. \end{cases}$$

Before proceeding with the discretization of the modified variational formulation, we need to define the global Lagrange functions and their restrictions to the subdomains, because they will play the role of the discrete test functions which are necessary for arriving to the final discrete system of equations. Towards that, we define:

$$v^l : \bar{\Omega} \to \Re, \quad l \in J^{\mathrm{G}},$$

$$v^l \in C^0(\bar{\Omega}),$$

$$v^l(\vec{x}_k) = \delta_k^l, \quad k, l \in J^{\mathrm{G}}.$$

Suppose now, that we have two specific grid points, namely, $\vec{x}_k, \vec{x}_l$, for some $k, l \in J^{\mathrm{G}}$. The first one belongs to a collection of subdomains, say, $\bar{\Omega}^m,\ m \in B_k \subseteq M$, while the second one belongs to the $\bar{\Omega}^m,\ m \in B_l \subseteq M$. We define the sets $C_k = M \setminus B_k$ and $C_l = M \setminus B_l$ to be the sets of the indices of the subdomains that do not contain $\vec{x}_k$ and $\vec{x}_l$, respectively. For a specific subdomain $\bar{\Omega}^m,\ m \in B_k \cap B_l$ (we silently suppose $B_k \cap B_l$ to be a nonempty set), there are correlations between the global indices $k, l \in J^{\mathrm{G}}$ and some local ones, say $\vec{i}_m, \vec{j}_m \in J$, defined by the relations:

$$k = G(m, \vec{i}_m),$$

$$l = G(m, \vec{j}_m).$$

We define the restriction of v^l in $\bar{\Omega}^m$, as the function $v^{l,m} \in C^0(\bar{\Omega}^m)$ which has the property $v^{l,m}(\vec{x}_k) = \delta^{\vec{j}_m}_{\vec{i}_m}$. Moreover, if $m \in C_l$ then $v^{l,m} = 0\ \forall \vec{x} \in \bar{\Omega}^m$, and if $m \in B_l$ but $m \in C_k$ then $v^{l,m}(\vec{x}_k) = 0$. Next, we use Lagrange functions with the property that $v^{l,m} \in P_N(\bar{D})$ if $m \in B_l$, and so we symbolically write:

$$v^{l,m} = v^{l,m}_N = \phi^{\vec{j}_m} \quad \text{if } m \in B_l.$$

Let us denote by the subscript N at the expressions of the differential forms, the approximations to these operators, which are obtained by replacing the exact derivatives by collocation ones. For convenience we use the notation $\langle f \rangle_{\vec{i}} = f(r_{i_1}, s_{i_2}),\ \vec{i} \in J$, and $\langle g \rangle_k = g(x_k, y_k), k \in J^{\mathrm{G}}$, for functions that are correspondingly defined on $\bar{D}$ and $\bar{\Omega}$. Then the discrete form of the modified variational formulation (5) is:

$$\left\| \begin{array}{l} u_N \in \hat{U}_N, \\ a_N(u_N, v^l_N) = b_N(v^l_N) \quad \forall v^l_N \in \hat{V}_N, \end{array} \right. \tag{6}$$

where the spaces of trial and test functions are, respectively, defined to be:

$$\hat{U}_N = \{u_N : \bar{\Omega} \to \Re, u_N \in C^0(\bar{\Omega}) \,|\, u^m_N \in P_N(\bar{D}) \text{ in } \bar{\Omega}^m,\ m \in M,\ \langle u_N \rangle_l = \langle g \rangle_l \text{ for } l \in J^{\mathrm{G}}_{b,\mathrm{D}}\},$$

$$\hat{V}_N = \{v^l_N : \bar{\Omega} \to \Re, v^l_N \in C^0(\bar{\Omega}), l \in J^{\mathrm{G}} \,|\, v^{l,m}_N \in P_N(\bar{D}) \text{ in } \bar{\Omega}^m,\ m \in M,\ v^l_N = 0 \text{ for } l \in J^{\mathrm{G}}_{b,\mathrm{D}}\}.$$

The linear forms that appear, are given by the following formulas:

$$a_N(u_N, v^l_N) = \sum_{m \in M} \left\{ \sum_{\vec{i} \in J} \left\langle L^m_N[u^m_N] \right\rangle_{\vec{i}} \langle \phi^{\vec{j}_m} \rangle_{\vec{i}} \left\langle \left| J^m_N \right| \right\rangle_{\vec{i}} \omega_{\vec{i}} + \sum_{p=1}^{4} \left(\sum_{\vec{i} \in J^p_b} \left\langle \vec{D}^m_{L_N}[u^m_N] \cdot \vec{N}^{m,p} \right\rangle_{\vec{i}} \langle \phi^{\vec{j}_m} \rangle_{\vec{i}} \omega^p_{\vec{i}} \right) \right\},$$

$$b_N(v^l_N) = \sum_{m \in M} \left\{ \sum_{\vec{i} \in J} \langle f^m \rangle_{\vec{i}} \langle \phi^{\vec{j}_m} \rangle_{\vec{i}} \left\langle \left| J^m_N \right| \right\rangle_{\vec{i}} \omega_{\vec{i}} + \sum_{p \in P^m} \left(\sum_{\vec{i} \in J^p_b} \langle h^m \rangle_{\vec{i}} \langle \| \vec{N}^{m,p} \| \rangle_{\vec{i}} \langle \phi^{\vec{j}_m} \rangle_{\vec{i}} \omega^p_{\vec{i}} \right) \right\}.$$

Eq. (6) is essentially different from the one encountered in classical spectral element algorithms, since it results from the discretization of the modified variational formulation (5), instead of the more commonly used form (4).

In the present work, we have utilized a Legendre method (see [1]), which means that the knots and weights defined above, are actually the ones of the Legendre–Gauss–Lobatto quadrature formula. Likewise, the Lagrange basis is defined on the Gauss–Lobatto points and the pseudospectral approximation of the continuous differential operators is generated by using Legendre collocation derivatives. We could have

used a Chebyshev method (similar to [9]), with weights given by the Clenshaw–Curtis integration formula, but we chose not to do so, in order to maintain maximum precision in the discrete evaluation of the integral forms.

In this section, we described the discrete multidomain version of the weak formulation of a general elliptic boundary value problem of second order. At the inner collocation points of each subdomain, the discrete equations obtained from this method are exactly the same as those obtained from the strong collocation formulation. The Dirichlet conditions are enforced exactly at each node of the Dirichlet boundary, in both methods. The differences between the weak and the strong formalisms, occur at the discrete equations for the nodes that lie on the Neumann boundary and on the interface between subdomains. At each node of the Neumann boundary, the boundary condition is specified up to a small constant (which vanishes as $N \to \infty$) multiplied by the pseudospectral residual at the same node. This weak imposition makes the utilization of Neumann boundary conditions as outflow conditions in Navier–Stokes simulations efficient, because there is no generation of numerically induced oscillations at the outflow boundary (see [29]). We also find that the type of interface condition which results from the weak formulation is clearer and has advantages at points where more than two subdomains meet, over the strong C^1 enforcement that is traditionally used with the strong formalism. Moreover, at corner points which belong to the Neumann boundary and also to two or more subdomains, the weak formalism faces no problem, while the condition that should be used with a strong collocation method is totally unclear. Before ending this section, we should mention that extreme caution is necessary when writing or programming the discrete equations at corner points, where contributions from the neighboring sides of the subdomains should be taken under consideration, according to the condition which has to be imposed on the particular point (Neumann condition, interface condition or both).

4.3. Weak formulation of the influence matrix method

In the numerical implementation of the present domain decomposition method, we wish to find a way to decouple the calculation of the solution in the subdomains from that on the interface and on a certain portion of the Neumann boundary. A commonly used algorithm for this kind of work at a discrete level, is the so-called influence matrix method. By utilizing such a technique, we are able to obtain the solution of the global system at the cost of two local solutions in each subdomain, plus a solution of a problem concerning the interface and boundary values we wish to uncouple. Further we require the calculation of the so-called discrete Green's functions and the formation of the influence matrix, which can be done once and for all in a preprocessing stage of the calculations. In this section, we set a weak formalism for this method, which fits well the above mentioned variational formulation of the boundary value problem and subsequently discuss some algorithmic aspects for a successful numerical implementation of this technique.

Let us say that a certain node belongs to the interface, if and only if it belongs to two or more subdomains and it is not contained in the Dirichlet portion of the boundary. We denote the set of scalar indices of these nodes by J_I^{G}, in the global numbering system. For reasons which concern the solution method of the linear algebraic systems resulting from the discrete version of the equations and that will become clear later, we wish to distinguish certain nodes that belong to the Neumann boundary and in order to do so, we indicate the set of their global indices as J_N^{G}. In the following discussion, we shall also need the union of the above sets, namely $J_S^{\mathrm{G}} = J_I^{\mathrm{G}} \cup J_N^{\mathrm{G}}$.

Let us define two discrete projection operators as:

$$T^S[e_N] = \langle e_N \rangle_l, \quad l \in J_S^{\mathrm{G}},$$

$$T^D[e_N] = \langle e_N \rangle_l, \quad l \in J_{b,\mathrm{D}}^{\mathrm{G}},$$

for every $e_N \in E_N = \{e_N : \bar{\Omega} \to \Re, e_N \in C^0(\bar{\Omega}) \,|\, e_N^m \in P_N(\bar{D}) \text{ in } \bar{\Omega}^m,\ m \in M\}$. Next, we perform a decomposition:

$$u_N = u_{\alpha,N} + u_{\beta,N}, \quad u_N \in \hat{U}_N, \tag{7}$$

such that:

$$T^S[u_{\alpha,N}] = 0,$$

$$T^S[u_{\beta,N}] = T^S[u_N],$$

$$T^D[u_{\alpha,N}] = T^D[u_N],$$

$$T^D[u_{\beta,N}] = 0.$$

From the linearity of the above operators as well as of the forms included in the variational formulation of the problem, we conclude that the original problem (6) is equivalent to the following decomposed form:

$$\left\| \begin{array}{l} u_{\alpha,N} \in \hat{U}_{N,\alpha}, \\ a_N(u_{a,N}, v_N^l) = b_N(v_N^l) \quad \forall v_N^l \in \hat{V}_{N,d}, \end{array} \right. \tag{8}$$

$$\left\| \begin{array}{l} u_{\beta,N} \in \hat{U}_{N,\beta}, \\ a_N(u_{\beta,N}, v_N^l) = 0 \quad \forall v_N^l \in \hat{V}_{N,d}, \end{array} \right. \tag{9}$$

along with conditions (7) and:

$$a_N(u_{\alpha,N}, v_N^l) + a_N(u_{\beta,N}, v_N^l) = b_N(v_N^l) \quad \forall v_N^l \in \hat{V}_{N,S}, \tag{10}$$

where:

$$\begin{aligned} \hat{U}_{N,\alpha} = \big\{ & u_{\alpha,N} : \bar{\Omega} \to \Re,\ u_{\alpha,N} \in C^0(\bar{\Omega}) \,|\, u_{\alpha,N}^m \in P_N(\bar{D}) \text{ in } \bar{\Omega}^m,\ m \in M, \\ & \langle u_{\alpha,N} \rangle_k = 0 \text{ for } k \in J_S^{\mathrm{G}}, \langle u_{\alpha,N} \rangle_k = \langle g \rangle_k \text{ for } k \in J_{b,\mathrm{D}}^{\mathrm{G}} \big\}, \end{aligned}$$

$$\begin{aligned} \hat{U}_{N,\beta} = \big\{ & u_{\beta,N} : \bar{\Omega} \to \Re,\ u_{\beta,N} \in C^0(\bar{\Omega}) \,|\, u_{\beta,N}^m \in P_N(\bar{D}) \text{ in } \bar{\Omega}^m,\ m \in M, \\ & \langle u_{\beta,N} \rangle_k = \langle u_N \rangle_k \text{ for } k \in J_S^{\mathrm{G}}, \langle u_{\beta,N} \rangle_k = 0 \text{ for } k \in J_{b,\mathrm{D}}^{\mathrm{G}} \big\}, \end{aligned}$$

$$\hat{V}_{N,d} = \big\{ v_N^l : \bar{\Omega} \to \Re, v_N^l \in C^0(\bar{\Omega}), l \in J^{\mathrm{G}} \,|\, v_N^{l,m} \in P_N(\bar{D}) \text{ in } \bar{\Omega}^m,\ m \in M,\ v_N^l = 0 \text{ for } l \in J_{b,\mathrm{D}}^{\mathrm{G}} \cup J_S^{\mathrm{G}} \big\},$$

$$\hat{V}_{N,S} = \big\{ v_N^l : \bar{\Omega} \to \Re, v_N^l \in C^0(\bar{\Omega}), l \in J_S^{\mathrm{G}} \,|\, v_N^{l,m} \in P_N(\bar{D}) \text{ in } \bar{\Omega}^m,\ m \in M \big\}.$$

At this point we can only solve problem (8), which amounts to computing uncoupled solutions of the restrictions $u_{\alpha,N}^m,\ m \in M$ within each subdomain. Problem (9) and conditions (10) are coupled together with the unknown nodal values $\langle u_N \rangle_k, k \in J_S^{\mathrm{G}}$. In order to solve the problem concerning the function $u_{\beta,N}$, we need to perform a further decomposition, namely:

$$u_{\beta,N} = \sum_{k \in J_S^{\mathrm{G}}} \langle u_N \rangle_k G_N^k, \tag{11}$$

where we have indicated as $G_N^k, k \in J_S^{\mathrm{G}}$, the discrete Green's functions (see [2]). Since the operator T^S is linear, we have:

$$T^S[u_N] = T^S[u_{\alpha,N} + u_{\beta,N}] = T^S[u_{\alpha,N}] + T^S[u_{\beta,N}] = T^S[u_{\beta,N}] = \sum_{k \in J_S^{\mathrm{G}}} \langle u_N \rangle_k T^S[G_N^k].$$

In view of the fact that:

$$T^S[u_{\beta,N}] = T^S[u_N] = \langle u_N \rangle_l, \quad l \in J_S^{\mathrm{G}},$$

we have:

$$T^S[G_N^k] = \langle G_N^k \rangle_l = \delta_l^k, \quad l, k \in J_S^{\mathrm{G}}. \tag{12}$$

Also:

$$T^D[u_{\beta,N}] = 0 \iff \sum_{k \in J_S^{\mathrm{G}}} \langle u_N \rangle_k T^D[G_N^k] = 0 \iff T^D[G_N^k] = 0 \iff \langle G_N^k \rangle_l = 0, \quad k \in J_S^{\mathrm{G}}, \ l \in J_{b,\mathrm{D}}^{\mathrm{G}}. \tag{13}$$

By inserting the expression (11) into problem (9) and by using (12) and (13), it is obvious that the discrete Green's functions for every $k \in J_S^{\mathrm{G}}$, are calculated by solving the following problems:

$$\left\| \begin{array}{l} G_N^k \in \hat{U}_{N,G}, \\ a_N(G_N^k, v_N^l) = 0 \quad \forall v_N^l \in \hat{V}_{N,d}, \ k \in J_S^{\mathrm{G}}, \end{array} \right.$$

where:

$$\hat{U}_{N,G} = \big\{ G_N^k : \bar{\Omega} \to \Re, \ G_N^k \in C^0(\bar{\Omega}) | G_N^{k,m} \in P_N(\bar{D}) \text{ in } \bar{\Omega}^m, \ m \in M, \\ \langle G_N^k \rangle_l = \delta_l^k \text{ for } l \in J_S^{\mathrm{G}}, \langle G_N^k \rangle_l = 0 \text{ for } l \in J_{b,\mathrm{D}}^{\mathrm{G}} \big\}.$$

So far, we have indicated the way to calculate all the discrete Green's functions and the particular solution $u_{\alpha,N}$. What remains to be found, is the set of the nodal values $\langle u_N \rangle_k, k \in J_S^{\mathrm{G}}$. This results from conditions (10) after using relation (11), which read:

$$\sum_{k \in J_S^{\mathrm{G}}} \langle u_N \rangle_k a_N(G_N^k, v_N^l) = b_N(v_N^l) - a_N(u_{\alpha,N}, v_N^l) \quad \forall v_N^l \in \hat{V}_{N,S},$$

where: $G_N^k \in \hat{U}_{N,G}, u_{\alpha,N} \in \hat{U}_{N,\alpha}$.
At the discrete level, the set of numbers:

$$[I_M]_{lk} = a_N(G_N^k, v_N^l), \quad k \in J_S^{\mathrm{G}}, \quad G_N^k \in \hat{U}_{N,G}, \quad v_N^l \in \hat{V}_{N,S}$$

constitute the components of the influence matrix.

There are many situations, met usually when dealing with time discretized evolution equations, when we need to solve elliptic boundary value problems, characterized by the same differential operator, at different time levels. This is actually the case, when solving the unsteady incompressible Navier–Stokes equations by a time-splitting scheme, as previously described. In such situations, it is wise to solve for the discrete Green's functions at a preprocessing stage of the calculations. Moreover, it is highly recommended to calculate the components of the influence matrix and store them in a convenient form depending on the solution method utilized, thus avoiding the great memory requirements needed for the storage of each one of the discrete Green's functions. By using such a technique, at every time level the given elliptic problem can be

decomposed into a series of solutions for the functions $u^m_{\alpha,N}$ in each subdomain (which are completely decoupled), plus a solution of the influence matrix problem and finally a series of solutions for the functions $u^m_N,\ m \in M$ with the correct boundary values imposed as Dirichlet conditions. This algorithm constitutes a very efficient way of dealing with time dependent equations whose discretization leads to linear elliptic boundary value problems to be solved at each time level and it is the one utilized in the subsequent Navier–Stokes simulations.

4.4. Aspects of the fully discretized form of the Navier–Stokes equations

As already mentioned, the temporal discretization scheme, decomposes the solution of the full Navier–Stokes equations into a sequence of elliptic problems to be solved at each time level. These problems are spatially approximated by the usage of the weak Legendre collocation spectral multidomain method, described in the preceeding sections. Here, we comment on some issues which arise from the implementation of the combination of the temporal and spatial schemes to the Navier–Stokes equations, as well as on the solution methods utilized to solve the final linear algebraic systems.

We begin by reporting some very important modifications which must be performed on the discrete forms of the elliptic problems, when dealing with axisymmetric flows. On the axis of symmetry ($y = 0$), boundary conditions should be specified so that the problem to be well defined. These conditions, namely "symmetry conditions", have the following form:

$$\frac{\partial u}{\partial n} = 0, \quad v = 0, \quad \frac{\partial p}{\partial n} = 0.$$

As we have mentioned, the weak imposition of Neumann boundary conditions at the discrete level, involves the calculation of the pseudospectral residual of the differential equations on the given grid node. In view of the fact that the differential equations governing both the velocity and pressure variables, are singular on the axis of symmetry, we need to modify the discrete variational statements. The new formulation of the linear forms occurring in the variational formulation of the boundary value problems, is:

$$\begin{aligned} a_N(u_N, v^l_N) = \sum_{m\in M} \Bigg\{ & \sum_{\vec{i}\in J} \langle (y^m)^c L^m_N[u^m_N] \rangle_{\vec{i}} \left\langle \phi^{\vec{j}_m} \right\rangle_{\vec{i}} \langle |J^m_N| \rangle_{\vec{i}} \omega_{\vec{i}} \\ & + \sum_{p=1}^{4} \left(\sum_{\vec{i}\in J^p_b} \left\langle (y^m)^c \vec{D}^m_{L_N}[u^m_N] \cdot \vec{N}^{m,p} \right\rangle_{\vec{i}} \left\langle \phi^{\vec{j}_m} \right\rangle_{\vec{i}} \omega^p_{\vec{i}} \right) \Bigg\}, \\ b_N(v^l_N) = \sum_{m\in M} \Bigg\{ & \sum_{\vec{i}\in J} \langle (y^m)^c f^m \rangle_{\vec{i}} \left\langle \phi^{\vec{j}_m} \right\rangle_{\vec{i}} \langle |J^m_N| \rangle_{\vec{i}} \omega_{\vec{i}} \\ & + \sum_{p\in P^m} \left(\sum_{\vec{i}\in J^p_b} \langle (y^m)^c h^m \rangle_{\vec{i}} \left\langle \| \vec{N}^{m,p} \| \right\rangle_{\vec{i}} \left\langle \phi^{\vec{j}_m} \right\rangle_{\vec{i}} \omega^p_{\vec{i}} \right) \Bigg\}, \end{aligned} \tag{14}$$

where c is the order of the pole $y = 0$ of the coefficient functions of each differential equation, namely one for the equations that govern the pressure and the u-component of the velocity vector, and two for the remaining equation governing the v-velocity component equation. Throughout this section, we indicate by l and $\vec{j}_m$ the global and local indices, respectively, that are correlated by the relation $l = G(m, \vec{j}_m)$, where m belongs to the set of indices of all the subdomains in which the certain node is contained. The test and trial

function spaces along with the boundary and initial conditions, remain unchanged by these modifications (in contrast with [27]). The above functionals are actually the ones that appear in the discrete form of the weak formulation of appropriately modified elliptic boundary value problems so that the desired elimination of the singularity has been accomplished. We included the equation for the radial velocity component in the above modifications, in case we need to impose a Neumann boundary condition on a node belonging to the axis of symmetry. With such a technique, the poles of the differential equations and of the boundary condition at the pressure predictor step, are efficiently eliminated. The same symmetry boundary conditions are prescribed at a two-dimensional symmetric flow, but in this case there is no singularity on the symmetry axis and the above treatment is no longer necessary.

At the interface nodes, where two or more subdomains meet and there is no Dirichlet boundary condition prescribed, the condition stemming from the weak formulation is not equivalent to the strong enforcement of C^1 continuity in all cases except in the limit $N \to \infty$. This fact has as a consequence the failure of the vorticity field to be globally continuous. Precisely, $\omega_N^m \in C^\infty(\Omega^m)$, $m \in M$, but $\omega_N \in L^2(\Omega)$ only. A more important implication, is that the corrected velocity field calculated by strong collocation at each discrete time level, is also discontinuous. Although this fact has not caused any problems in any of the Navier–Stokes simulations, we used in some of them, the method of weak collocation updating (see [5]) as an attempt to improve the quality of the results. For the sake of completeness, we shall briefly describe its implementation. Suppose that we have a relationship of the form:

$$u = \bar{u} + \tilde{u},$$

where $\bar{u} \in C^0(\bar{\Omega})$ and $u, \tilde{u} \in L^2(\Omega)$. After multiplying by a suitably integrable function and integrating, we get:

$$\int_\Omega \int uv = \int_\Omega \int \bar{u}v + \int_\Omega \int \tilde{u}v \quad \text{for } v \in L^2(\Omega),$$

which is equivalent to:

$$\sum_{m\in M} \int_{\Omega^m} \int u^m v^m = \sum_{m\in M} \int_{\Omega^m} \int \bar{u}^m v^m + \sum_{m\in M} \int_{\Omega^m} \int \tilde{u}^m v^m.$$

Suppose, now, that we have a certain node $\vec{x}_l$ for some $l \in J_I^G$, which belongs to the interface. This node belongs to a set of subdomains $\bar{\Omega}^m$, $m \in B_l \subseteq M$. The above equation, written in discrete form for this specific node, becomes (by using the properties of the Lagrangian base):

$$\sum_{m\in B_l} \langle u_N^m \rangle_{\vec{j}_m} \langle |J_N^m| \rangle_{\vec{j}_m} \omega_{\vec{j}_m} = \sum_{m\in B_l} \langle \bar{u}_N^m \rangle_{\vec{j}_m} \langle |J_N^m| \rangle_{\vec{j}_m} \omega_{\vec{j}_m} + \sum_{m\in B_l} \langle \tilde{u}_N^m \rangle_{\vec{j}_m} \langle |J_N^m| \rangle_{\vec{j}_m} \omega_{\vec{j}_m}.$$

Since we want $u \in C^0(\bar{\Omega})$, we have:

$$\left(\sum_{m\in B_l} \langle |J_N^m| \rangle_{\vec{j}_m} \omega_{\vec{j}_m} \right) \langle u_N^m \rangle_l = \left(\sum_{m\in B_l} \langle |J_N^m| \rangle_{\vec{j}_m} \omega_{\vec{j}_m} \right) \langle \bar{u}_N^m \rangle_l + \sum_{m\in B_l} \langle \tilde{u}_N^m \rangle_{\vec{j}_m} \langle |J_N^m| \rangle_{\vec{j}_m} \omega_{\vec{j}_m}$$

and so:

$$\langle u_N^m \rangle_l = \langle \bar{u}_N^m \rangle_l + \frac{\sum_{m\in B_l} \langle \tilde{u}_N^m \rangle_{\vec{j}_m} \langle |J_N^m| \rangle_{\vec{j}_m} \omega_{\vec{j}_m}}{\sum_{m\in B_l} \langle |J_N^m| \rangle_{\vec{j}_m} \omega_{\vec{j}_m}}$$

for every $m \in B_l$. This procedure is repeated for every node which belongs to the interface, so that at the end, the function u to be globally continuous.

Next, a few comments are deserved by the incompressibility constraint. In every subdomain, the condition $\nabla \cdot \vec{u} = 0$ is met at every inner collocation node in the strong collocation sense at each time level. Since a problem dependent boundary condition is prescribed at the Dirichlet boundary for the pressure, the final velocity field fails to be solenoidal locally. At a point belonging to the interface, say $\vec{x}_l, l \in J_I^{\mathrm{G}}$ which belongs to the family of subdomains $\{\overline{\Omega}^m\}_{m\in B_l}$, we apply (along with the continuity condition which is implemented implicitly by the influence matrix method) the interface condition resulting from the weak formulation of the problem. This means that we cannot impose the conditions of incompressibility $\nabla \cdot \vec{u}_N^m = 0, m \in B_l$ in a strong collocation form, so such conditions can only be fulfilled at the limit of infinite resolution. In order to clarify the above allegations, we proceed by first applying the divergence operator on the corrected velocity field:

$$D[\vec{u}^{n+1}] = D[\vec{u}^*] - D[\vec{G}[\tilde{p}^{n+1}]].$$

After multiplication by a suitable test function $v \in L^2(\Omega)$, and after taking under consideration the modifications for the axisymmetric case, we integrate over Ω and get:

$$\int_\Omega \int y^a D[\vec{u}^{n+1}]v = \int_\Omega \int y^a D[\vec{u}^*]v - \int_\Omega \int y^a D[\vec{G}[\tilde{p}^{n+1}]]v,$$

where $a = 0, 1$ for two-dimensional and axisymmetric flows, respectively. In order to be consistent with our previous definitions, we indicate the differential operator and the right hand side function that appear in the pressure corrector boundary value problem as: $L[\tilde{p}^{n+1}] = -D[G[\tilde{p}^{n+1}]]$ and $f = -D[\vec{u}^*]$. We incorporate the domain decomposition idea and so the above relationship transforms into:

$$\sum_{m\in M}\left\{\int_{\Omega^m}\int (y^m)^a D^m[\vec{u}^{n+1,m}]v^m\right\} = \sum_{m\in M}\left\{\int_{\Omega^m}\int (y^m)^a L^m[\tilde{p}^{n+1,m}]v^m - \int_{\Omega^m}\int (y^m)^a f^m v^m\right\}.$$

If we suppose that $v \in \hat{V}$ and we use the variational formulation of the pressure corrector equation to manipulate the right-hand side, we result at:

$$\sum_{m\in M}\left\{\int_{\Omega^m}\int (y^m)^a D^m[\vec{u}^{n+1,m}]v^m\right\} = \sum_{m\in M}\left\{\int_{\Gamma_N^m} (y^m)^a h^m v^m - \oint_{\partial\Omega^m} (y^m)^a \left(\vec{D}_L^m[\tilde{p}^{n+1,m}]\cdot\vec{n}^m\right)v^m\right\}.$$

By following a similar procedure, as we already have in the proceeding sections, we arrive to the following discretized form:

$$\begin{aligned}
&\sum_{m\in M}\left\{\sum_{\vec{i}\in J}\left\langle (y^m)^a D_N^m[\vec{u}_N^{n+1,m}]\right\rangle_{\vec{i}}\left\langle \phi^{\vec{j}_m}\right\rangle_{\vec{i}}\langle |J_N^m|\rangle_{\vec{i}}\omega_{\vec{i}}\right\}\\
&\quad = \sum_{m\in M}\left\{\sum_{p\in P^m}\left(\sum_{\vec{i}\in J_b^p}\langle (y^m)^a h^m\rangle_{\vec{i}}\left\langle \|\vec{N}^{m,p}\|\right\rangle_{\vec{i}}\langle \phi^{\vec{j}_m}\rangle_{\vec{i}}\omega_{\vec{i}}^p\right)\right.\\
&\qquad \left. - \sum_{p=1}^{4}\left(\sum_{\vec{i}\in J_b^p}\left\langle (y^m)^a \vec{D}_{L_N}^m[\tilde{p}_N^{n+1,m}]\cdot\vec{N}^{m,p}\right\rangle_{\vec{i}}\left\langle \phi^{\vec{j}_m}\right\rangle_{\vec{i}}\omega_{\vec{i}}^p\right)\right\},
\end{aligned} \tag{15}$$

which applies for test functions that belong to an appropriate function space. $D_N^m[\cdot]$ is the discrete divergence operator in subdomain Ω^m, and all the remaining notations correspond to the discrete variational form of the pressure corrector equation. So, for a certain node $\vec{x}_l$ for some $l \in J^{\mathrm{G}} \setminus J_{b,\mathrm{D}}^{\mathrm{G}}$, relation (15) expresses the

necessary condition which the discrete divergence of velocity is forced to fulfill, by the weak approximation method. It is obvious that when $\vec{x}_l$ is an internal node of a certain subdomain, then the discrete divergence is equal to zero, but when $\vec{x}_l$ belongs to the interface or to the pressure Neumann boundary (or to both), then the velocity field fails to be solenoidal at the neighborhood of that node, although the spectral method guarantees an exponential decay of the absolute value of the discrete velocity divergence. For axisymmetric problems, we are not provided with any information concerning the nodes on the axis of symmetry, where the discrete divergence itself is singular. Finally, we need to point out that if we use weak collocation updating, locally at the interface nodes, then the divergence of velocity differs from zero also at the inner collocation nodes of each subdomain.

When we face a Dirichlet problem for the velocity, then we have a Neumann problem for the pressure which is not well posed. In order to render a unique solution, we drop one collocation condition at a point and instead we fix the discrete mean value of the pressure to be equal to zero, namely:

$$\sum_{m\in M}\left(\sum_{\vec{i}\in J}\langle p_N^m\rangle_{\vec{i}}\langle|J_N^m|\rangle_{\vec{i}}\omega_{\vec{i}}\right)=0.$$

In the present work, the usual (convective) form of the advection terms is discretized. There has not been found any form of instability stemming from this usage even for marginal resolution simulations (see [30,31]). We have, also, discretized the skew-symmetric form of the operator which produced the same results, so we decided not to implement it finally, because of the larger number of operations needed to calculate the discrete terms.

The only disadvantage of the application of the weak collocation method and the chosen projection method for the temporal approximation, we detected, is an instability which occurs when significantly decreasing the time step, while keeping the spatial resolution fixed. Such a behavior is still present when a single domain method is used, but it is not observed when a strong collocation approximation is utilized. Therefore, we are led to believe that this instability stems from the weak imposition of the Neumann boundary conditions at the pressure calculation steps of the time splitting technique. To be more precise, the weak imposition of the homogeneous Neumann boundary condition at the pressure correction step causes the failure of the final velocity field to satisfy the condition $\vec{u}^{n+1}\cdot\vec{n}=\vec{g}^{n+1}\cdot\vec{n}$ on the velocity Dirichlet boundary $\Gamma_{\mathrm{D}}^{u}\cap\Gamma_{\mathrm{D}}^{v}$. Then, an error occurs in evaluating the right-hand side of the Neumann boundary condition at the pressure predictor step, which is large when Δt is small and consequently destabilizes the system. The substitutions $\vec{u}^{n}\cdot\vec{n}=\vec{g}^{n}\cdot\vec{n}$ and $\vec{u}^{n-1}\cdot\vec{n}=\vec{g}^{n-1}\cdot\vec{n}$ at the first term of the right hand side of the Neumann boundary condition at the pressure predictor step completely eliminate this instability for steady state problems and considerably improve the behavior of the method at time dependent simulations, but may induce larger pressure errors especially at poorly and moderately resolved calculations. Such an instability appears in a much weaker form even when we use a different time splitting scheme (similar to the one proposed in [13]) where the pressure and velocity steps are inverted. This method provides accurate results but presents the drawbacks of larger pressure and divergence errors. For well-resolved flows, the time step that results in the destabilization of the system in our simulations was found to be very small (comparable to the machine precision), practically unusable for actual computations. Simultaneous increase of the spatial resolution, when significantly decreasing the time step, is strongly recommended to avoid this situation with the weak formalism.

Before we end this section, it is necessary to say a few words about the solution method employed to solve the linear algebraic systems resulting from the discretization of the elliptic problems. In all simulations and subdomain topologies, the influence matrix problems were solved at each time step by a standard LU-factorization method, where the influence matrices corresponding to each problem (velocity or pressure) were factorized and stored in a preprocessing stage. As far as the local problems in the individual subdomains are concerned, we made a distinction between subdomains with curvilinear boundaries (or linear

but not orthogonal ones), in which the equations were solved by LU-factorization combined with diagonal scaling (see [19]), and orthogonal subdomains where we used the tensor-product diagonalization algorithm (see [1,2,6,27]). The standard form of the matrix-diagonalization method needs Dirichlet boundary conditions in order to work and that is the reason why we included some of the nodes belonging to the Neumann boundary, in the influence matrix problems. This means that at the orthogonal subdomains, the Neumann boundary conditions were converted to Dirichlet ones through the influence matrix technique so that the diagonalization method to be applicable. The combination of the LU-factorization and matrix-diagonalization methods was found to be very efficient numerically, as long as the number of the non-orthogonal subdomains was kept at a low level. The resulting simulation code is so efficient that all of the results to be shown in this paper were obtained on a 2.4 GHz Pentium Personal Computer.

5. Stokes and Navier–Stokes solutions

In this section, we concern ourselves with solutions of the Stokes and the Navier–Stokes equations, by using the temporal and spatial approximation methods described above. Spatial spectral accuracy as well as temporal second order accuracy is confirmed. First, we check the monodomain algorithm at a boundary value problem with a nonempty Neumann boundary set. In order to do this, we use the Hamel flow test problem, in two different domain configurations. Then, we study the convergence properties of the scheme in a complex geometry problem, namely the Wannier flow, and examine the performance of the computer codes in curvilinear geometries. Subsequently, we proceed by computing the steady state solution of the Kovasznay problem, which is the first full Navier–Stokes simulation at low Reynolds number that we perform. To show the ability of the method to handle unstructured domain decomposed topologies and also to study the temporal properties of the algorithm, we use the well known transient Taylor–Green vortex solution. So far, we have dealt with analytical solutions of model problems. Next, we present the steady state solution of the regularized lid driven cavity problem, while comparing our results with other published ones, and finally perform an axisymmetric simulation in a stenosed pipe.

Before we actually proceed with the specific test cases, we should comment, for a while, on the norms used for convergence to steady state and for comparisons to the analytical solutions. When solving for a steady state of a function (say u) by means of a time integration method, we march in pseudotime and hope that by adjusting the spatial and temporal resolutions according to the specified data of the problem, we shall end with convergence. We set the sequence $u^n = u(\vec{x}, n \cdot \Delta t),\ \vec{x} \in \Omega,\ n = 0, 1, \ldots$, and we accept that it is a Cauchy sequence in a Banach space $X(\Omega)$, namely, for each positive integer $\varepsilon > 0$, there exists an integer $N = N(\varepsilon) > 0$, such that the norm $\|u^k - u^l\|_X$ between any two elements of the sequence is smaller than ε, provided both k, l are larger than N. We consider the case when the two elements of the sequence are two successive approximations of the steady-state solution ($k = n + 1, l = n$), so by determining the Banach space X (and consequently its norm $\|\cdot\|_X$) we can study the convergence of the method in pseudotime. In the subsequent simulations, we have utilized the discrete forms of the following norms:

$$X(\Omega) = L^\infty(\Omega): \quad \|u\|_{L^\infty} = \sup_{\vec{x} \in \Omega} \left| u(\vec{x}) \right|,$$

$$X(\Omega) = L^2(\Omega): \quad \|u\|_{L^2} = \left\{ \int_\Omega \int |u|^2 \right\}^{1/2},$$

$$X(\Omega) = H^1(\Omega): \quad \|u\|_{H^1} = \left\{ \int_\Omega \int \left[|u|^2 + \left(\frac{\partial u}{\partial x} \right)^2 + \left(\frac{\partial u}{\partial y} \right)^2 \right] \right\}^{1/2},$$

where the derivatives that appear are considered in the distributional sense. The same norms were used in order to compare the computed (u_c) to the exact (u_e) solutions and in this case we computed the form: $\|u_c - u_e\|_X$. For steady-state problems, u_c is the final converged function, while for transient problems, the variables u_c, u_e can be evaluated at any time level, we wish the comparison to be performed.

5.1. Hamel flow

We begin the numerical tests by employing the monodomain method, in order to solve the Stokes flow in a two-dimensional symmetric divergent channel. This problem was first solved by Hamel and the exact solution reads (see [32]):

$$u_e(x,y) = \frac{Qx}{x^2+y^2}\left(\frac{x^2-y^2}{x^2+y^2} - \cos(2a)\right)\frac{1}{\sin(2a) - 2a\cos(2a)},$$

$$v_e(x,y) = \frac{Qy}{x^2+y^2}\left(\frac{x^2-y^2}{x^2+y^2} - \cos(2a)\right)\frac{1}{\sin(2a) - 2a\cos(2a)},$$

where Q is the flow rate, $2a$ is the total angle of the diverted channel and (x,y) are the spatial coordinates in a Cartesian frame of reference. The problem was solved for two different domain configurations with angles $a = 5°$ and $a = 20°$, respectively. The meshes, for a polynomial order of $N = 11$, are presented in Fig. 1. The computational region was bounded by the lines: $y = 0,\ x = 1.5,\ y = x\tan(a)$, and $x = 1.0$. At the bottom of the domain, we imposed symmetry boundary conditions, while on the rest of the boundary, we set the analytical solution as a Dirichlet condition. For our simulations, we have used $Q = 2,\ N = 0, Re = 1$ (since we are dealing with Stokes flow) and zero initial conditions for the velocity components. The convergence of the spatial error is exponential as demonstrated in Figs. 2 and 3. Here, and in all subsequent simulations, we have set $f = 0$ (null body force term), and whenever we tested the spatial accuracy of the method, we ensured that the value of the time step was kept small enough in order to make the temporal discretization errors negligible.

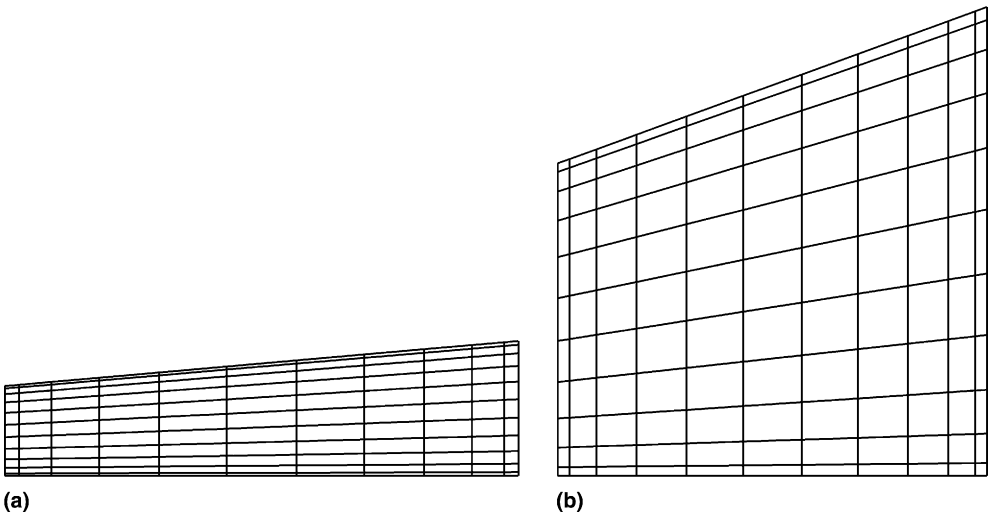

Fig. 1. Grids for the Hamel flow computation with (a) $a = 5°$ (b) $a = 20°$.

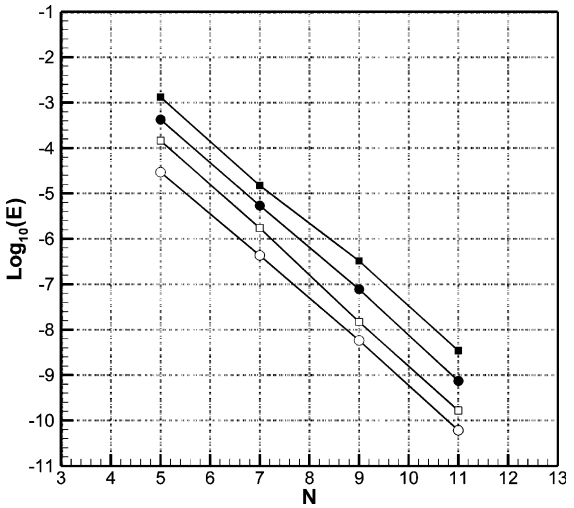

Fig. 2. Convergence plot for the Hamel flow with $a = 5°$: ■, $E = \|u_c - u_e\|_{L^\infty}$; ●, $E = \|v_c - v_e\|_{L^\infty}$; □, $E = \|u_c - u_e\|_{L^2}$; ○, $E = \|v_c - v_e\|_{L^2}$.

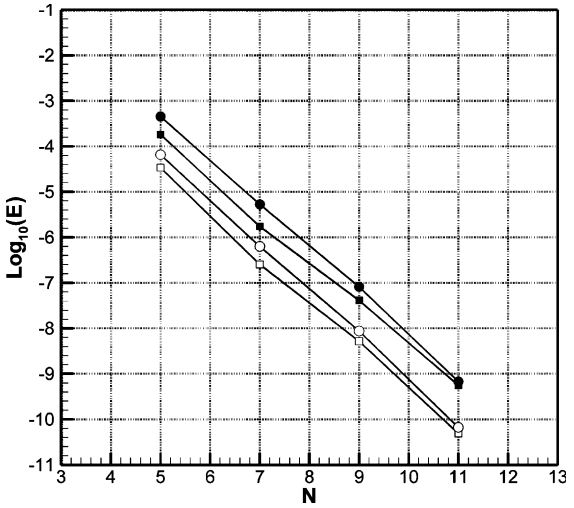

Fig. 3. Convergence plot for the Hamel flow with $a = 20°$: ■, $E = \|u_c - u_e\|_{L^\infty}$; ●, $E = \|v_c - v_e\|_{L^\infty}$; □, $E = \|u_c - u_e\|_{L^2}$; ○, $E = \|v_c - v_e\|_{L^2}$.

5.2. Wannier flow

As a second test case, we considered the steady Stokes flow past a rotating circular cylinder close to a moving wall. By the aid of this problem, we were able to study the performance of the multidomain method in a curvilinear topology. This problem has been used in the past for code verification purposes (for example see [13,15,32–34]). The exact solution is given by the relations:

$$u_e(x,y) = U - 2(a_1 + a_0 y_1)\left(\frac{s+y_1}{k_1} + \frac{s-y_1}{k_2}\right) - a_0 \ln\frac{k_1}{k_2} - \frac{a_2}{k_1}\left(s + y_2 - \frac{(s+y_1)^2 y_2}{k_1}\right) - \frac{a_3}{k_2}\left(s - y_2 + \frac{(s-y_1)^2 y_2}{k_2}\right),$$

$$v_e(x,y) = \frac{2x}{k_1 k_2}(a_1 + a_0 y_1)(k_2 - k_1) - \frac{x a_2 (s+y_1) y_2}{k_1^2} - \frac{x a_3 (s-y_1) y_2}{k_2^2},$$

where:

$$s^2 = d^2 - r^2, \quad \Gamma = \frac{d+s}{d-s}, \quad a_0 = \frac{U}{\ln \Gamma}, \quad a_1 = -d\left(a_0 + \frac{r^2\omega}{2s}\right),$$

$$a_2 = (d+s)\left(a_0 + \frac{r^2\omega}{2s}\right), \quad a_3 = (d-s)\left(a_0 + \frac{r^2\omega}{2s}\right), \quad y_1 = y + d,$$

$$y_2 = 2y_1, \quad k_1 = x^2 + (s+y_1)^2, \quad k_2 = x^2 + (s-y_1)^2.$$

The cylinder radius was presumed $r = 0.25$, the distance from the center of the cylinder to the moving wall was $d = 0.5$, the velocity of the moving wall was $U = 1$ and the angular velocity of the rotating cylinder (in a counter clockwise sence) was $\omega = 2$. The spatial domain was $\Omega = (-1.5, 3.0) \times (-0.5, 2.5) - N(0, 0.25)$, where $N(0, 0.25)$ is the circle of radius 0.25 with its center at 0.0. The detailed grid, for $N = 11$, is displayed in Fig. 4. In all our simulations we have used 28 subdomains and Dirichlet boundary conditions. The initial conditions used for the velocity components were zero in some simulations and equal to the exact steady state solution (which is not the solution of the discrete system of equations) in some others. The convergence to steady state proves the good behavior of the method to different but compatible initial conditions. The results of the *p*-convergence studies of the flow are presented in Fig. 5. Very good agreement in the results is found by comparison with [33], although Sherwin and Karniadakis have used more subdomains in their spectral element simulations. At this point, we feel necessary to say that the combination of the LU-factorization technique at the curvilinear subdomains around the cylinder, with the matrix-diagonalization technique, used for all the other orthogonal subdomains, was confirmed to be very efficient. Moreover, at

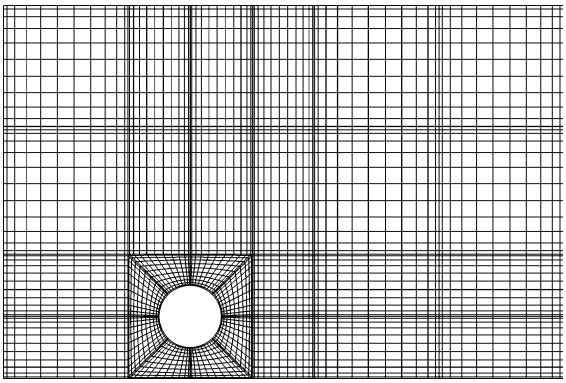

Fig. 4. Grid for the Wannier flow simulation.

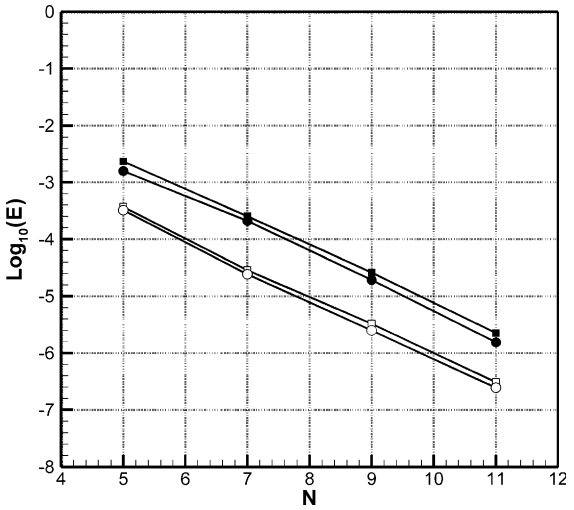

Fig. 5. Convergence plot for the Wannier flow: ■, $E = \|u_c - u_e\|_{L^\infty}$; ●, $E = \|v_c - v_e\|_{L^\infty}$; □, $E = \|u_c - u_e\|_{L^2}$; ○, $E = \|v_c - v_e\|_{L^2}$.

corner points where three or five subdomains meet, the present weak formulation faces no difficulty in contrast with the strong form of the spatial approximation method.

5.3. Kovasznay flow

In this section, we test our numerical method in the context of Navier–Stokes computations. The Kovasznay flow field represents the steady low speed flow of a viscous fluid past an array of cylinders. It is given by the following relationships:

$$u_e(x,y) = 1 - e^{\lambda x}\cos(2\pi y),$$

$$v_e(x,y) = \frac{\lambda}{2\pi}e^{\lambda x}\sin(2\pi y),$$

where $\lambda = Re/2 - ((Re^2/4) + 4\pi^2)^{1/2}$. The equations were solved in the domain $\Omega = (-0.5, 1.0) \times (-0.5, 1.5)$ and the finest mesh is shown in Fig. 6. In our simulations, we used 16 subdomains, Dirichlet boundary conditions for the velocity components and a Reynolds number equal to 40. Spectral accuracy is demonstrated for this laminar solution in Fig. 7.

5.4. Taylor–Green vortex

We proceed with a transient flow problem, namely the Taylor–Green decaying vortex system. This test case helped us study the temporal accuracy of our numerical method and has been also used in [5,14], among others. The spatial solution domain was $\Omega = (0, \pi)^2$ and the analytical solution of the Navier–Stokes equations, with $Re = 1$, for this problem read:

$$u_e(x,y,t) = -\cos(x)\sin(y)e^{-2t},$$

$$v_e(x,y,t) = \sin(x)\cos(y)e^{-2t},$$

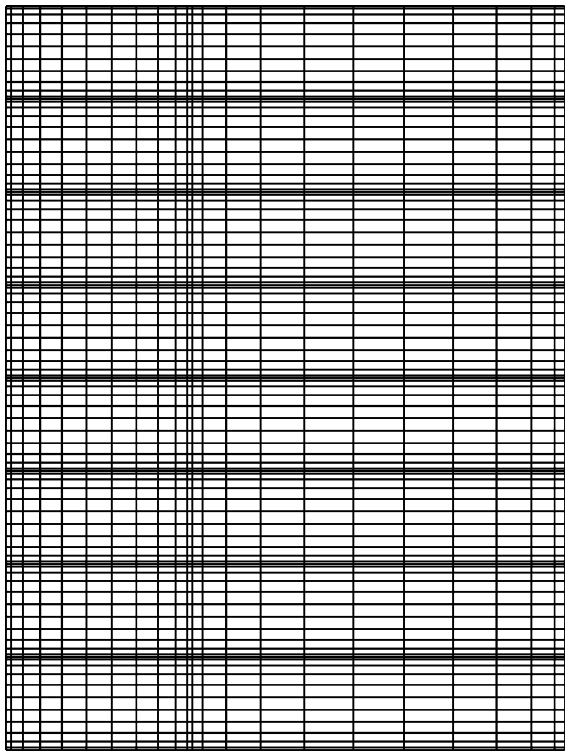

Fig. 6. Grid for the Kovasznay flow computation.

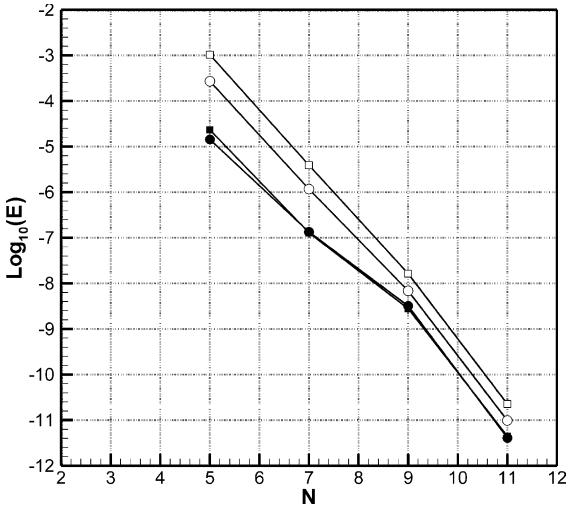

Fig. 7. Convergence plot for the Kovasznay flow: ■, $E = \|u_c - u_e\|_{L^\infty}$; ●, $E = \|v_c - v_e\|_{L^\infty}$; □, $E = \|u_c - u_e\|_{H^1}$; ○, $E = \|v_c - v_e\|_{H^1}$.

$$p_e(x,y,t) = -\frac{1}{4}(\cos(2x) + \cos(2y))e^{-4t}.$$

First, we used a four subdomain partition of the computational domain and concerned ourselves with spatial accuracy. To this end, we used a time step $\Delta t = 10^{-5}$ and computed the discrete H^1-norms after 100 time steps. The structured grid, for $N = 14$, is shown in the first part of Fig. 8, while the convergence plot in Fig. 9. From the diagrams, it is obvious that the errors in the velocity components are graphically indistinguishable. Moreover, we confirmed the success of our first-order accurate time starting scheme, since it did not cause any increase of the error in the first steps of this transient simulation. In order to measure the time accuracy of the method, we sustained the same subdomain topology but used a polynomial order equal to 14 in each subdomain and evaluated the discrete L^2-norm of the error after one time unit. The

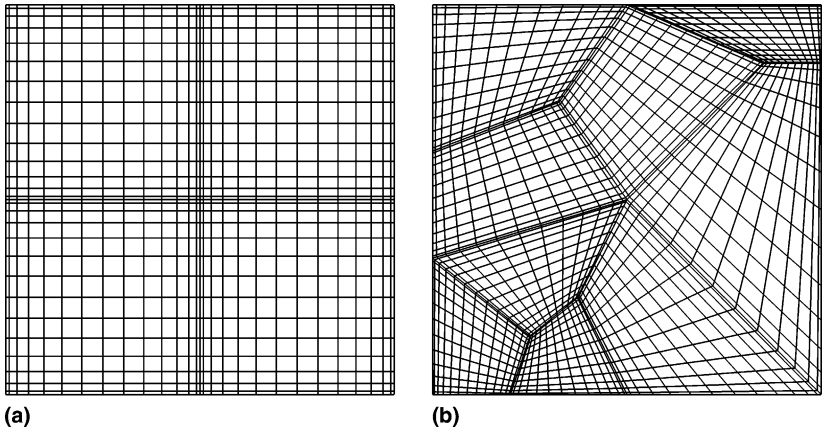

Fig. 8. Structured (a) and unstructured (b) grids for the Taylor–Green vortex simulation.

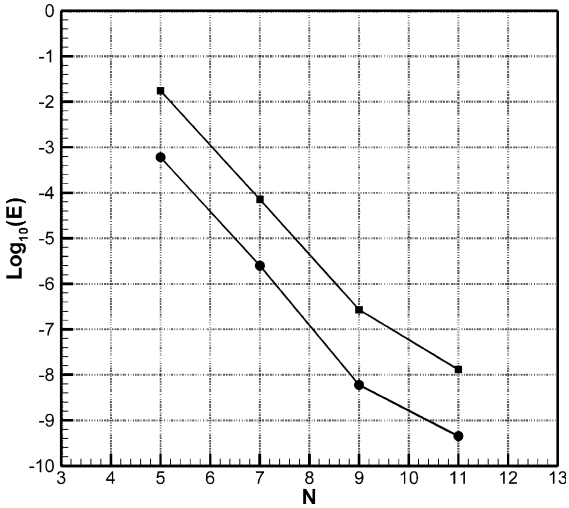

Fig. 9. Convergence plot for the structured configuration of the Taylor–Green vortex problem: ▲, $E = \|u_c - u_e\|_{H^1}$; ●, $E = \|v_c - v_e\|_{H^1}$; ■, $E = \|p_c - p_e\|_{H^1}$.

Table 1
Temporal accuracy results for the Taylor–Green vortex problem

Δt	$\|u_c - u_e\|_{L^2}$	$\|v_c - v_e\|_{L^2}$	$\|p_c - p_e\|_{L^2}$
10^{-1}	5.15×10^{-4}	5.17×10^{-4}	3.59×10^{-3}
10^{-2}	1.67×10^{-6}	1.67×10^{-6}	4.21×10^{-5}
10^{-3}	1.36×10^{-8}	1.35×10^{-8}	4.42×10^{-7}
10^{-4}	1.32×10^{-10}	1.32×10^{-10}	4.44×10^{-9}
10^{-5}	1.28×10^{-12}	1.28×10^{-12}	3.93×10^{-11}

results are displayed in Table 1. Second order temporal accuracy is demonstrated for all of the flow variables.

Next, we solved the Taylor–Green vortex problem on an unstructured subdomain configuration shown in the second part of Fig. 8. Exponential convergence was achieved for both the velocity and pressure variables in the H^1-norm, as presented in Fig. 10. It is obvious that by using the weak collocation method, we have overcome many of the restrictions of the traditional strong formulation and extended the applicability of patching collocation methods to more complicated geometries. In all the above simulations of the Taylor–Green vortex system, we used the exact solution as initial condition as well as time-dependent Dirichlet boundary conditions.

5.5. Regularized lid driven cavity flow

The regularized lid driven cavity flow test case is very popular among spectral modelers. Since there is no analytical solution available, we compare our computational results with the ones produced by other authors (see [16,35]). We refer directly to [16] and references therein.

In our work, we calculated only steady flows, for two different Reynolds numbers. The spatial domain was $\Omega = (0,1)^2$ and the boundary conditions read:

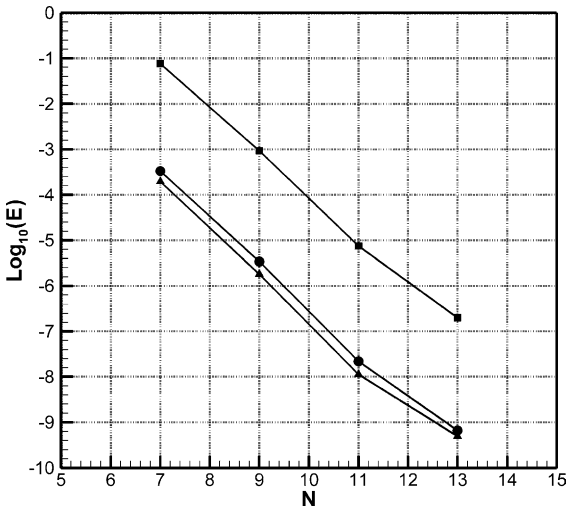

Fig. 10. Convergence plot for the unstructured configuration of the Taylor–Green vortex problem: ▲, $E = \|u_c - u_e\|_{H^1}$; ●, $E = \|v_c - v_e\|_{H^1}$; ■, $E = \|p_c - p_e\|_{H^1}$.

$$u(x,1) = -16x^2(1-x)^2,$$

$$v(x,1) = 0$$

for the top lid and $u = v = 0$, for all the other stationary walls. In all simulations, we started with zero initial conditions for the velocity field. The comparisons were carried out on the extremum values of vorticity at the moving lid, from the spectral solution interpolated on a uniform 201×201 grid, along with the location of that vorticity value computed. We denote these variables by $M = \max_{x\in[0,1]} |\omega(x,1)|$ and x_M. We used a four subdomain configuration of equal area, and the results along with the time steps utilized at each computation are presented in Tables 2 and 3, for Reynolds numbers $Re = 100$ and 400, respectively. For comparison, the results of the single domain method are reported in Table 4. We see a very good agreement with the results of Hugues et al. despite the fact that they used one domain and a strong Chebyshev collocation approximation. The overall conclusions we drew from this test case, is the spectral convergence of vorticity, which is a secondary variable computed from the velocity field, the robustness of the method as far as the impulsive starting of the lid is concerned, along with the observation that the usage of weak collocation updating upgraded the already stable behavior of the method at marginal resolutions.

5.6. Axisymmetric flow inside a stenosed pipe

In this last problem, we face a more realistic situation, namely the fluid flow through an axisymmetric pipe presenting a constriction. This problem has already been considered in [36], where it was treated by

Table 2
Simulation parameters and characteristic flow variables for the regularized lid driven cavity flow at $Re = 100$ with the four subdomain configuration

N	Δt	M	x_M
8	0.050	13.6130	0.616
10	0.050	13.4752	0.621
12	0.020	13.4500	0.621
16	0.020	13.4440	0.621

Table 3
Simulation parameters and characteristic flow variables for the regularized lid driven cavity flow at $Re = 400$ with the four subdomain configuration

N	Δt	M	x_M
8	0.020	25.7757	0.601
10	0.020	25.5905	0.616
12	0.020	25.1141	0.626
16	0.010	24.9279	0.626

Table 4
Simulation parameters and characteristic flow variables for the regularized lid driven cavity flow with the one domain configuration

Re	N	Δt	M	x_M
100	32	0.050	13.4447	0.620
400	32	0.027	24.9107	0.630

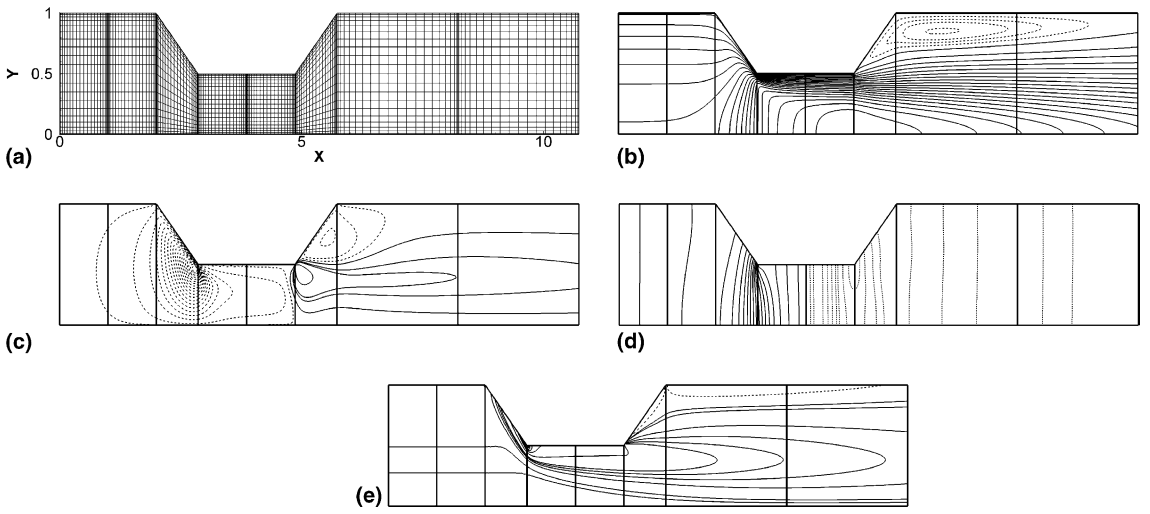

Fig. 11. Axisymmetric stenosed pipe flow computation (a) grid, (b) axial velocity component, (c) radial velocity component, (d) pressure, (e) vorticity.

finite volume methods utilizing either pseudocompressibility or pressure correction temporal discretization schemes. In our simulation, we used a high resolution mesh, part of which is shown in Fig. 11, while the actual dimensionless streamwise coordinate extended up to 25.73. The boundary conditions used were no-slip conditions for the velocity components on the upper boundary, symmetry conditions on the lower boundary, while on the left boundary we used the following inflow conditions:

$$u = 1 - y^2, \quad v = 0,$$

and on the right computational boundary we imposed custom outflow boundary conditions:

$$\frac{\partial u}{\partial n} = 0, \quad v = 0, \ p = 0.$$

The computations were started from rest and were performed for a Reynolds number of 100. The overall topology was comprised by 13 subdomains. Simulations were conducted with various polynomial orders in each subdomain. Almost identical results (within graphical accuracy) were found when $N = 16$ and $N = 20$, so for the sake of brevity we report only the results produced by the higher resolution simulation. Contour plots of the basic flow fields are presented in Fig. 11. We observe the vorticity to be C^1 continuous across the subdomain boundaries, although the spatial approximation method does not even ensure the C^0 continuity of this variable.

For validation purposes, the solution of this last test problem was also obtained by a simulation code which utilized a pseudocompressibility time integration method along with a flux vector splitting finite volume technique for the spatial discretization (similar to [36]). In Fig. 12 we show the axial distribution of pressure and in Fig. 13 several axial velocity profiles around the stenotic part of the pipe are displayed, as calculated by the two different methods. We denote by $D_u^{x_0}$ the maximum absolute value of the difference between the axial velocity components as computed by the two methodologies, over all the nodes of the finite volume grid with constant axial coordinate $x = x_0$. The values $D_v^{x_0}$ and $D_p^{x_0}$ are defined in a similar way for the radial velocity component and pressure, respectively. These differences, which are calculated after a suitable projection of the spectral solution (with $N = 20$) on the 443×35 grid used by the finite volume

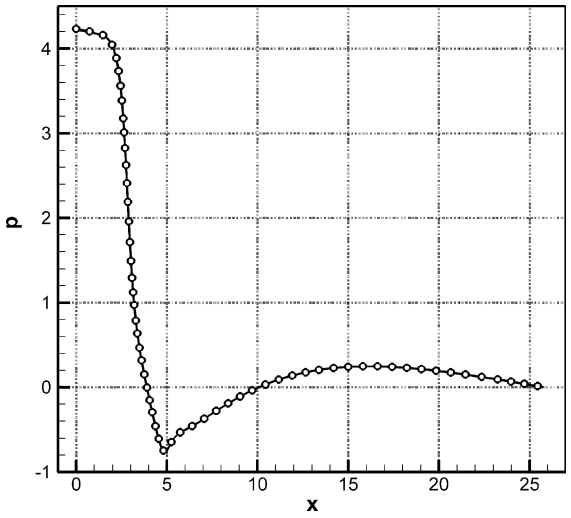

Fig. 12. Axial distribution of the pressure variable for the axisymmetric stenosed pipe. Continuous line: spectral solution. Dashed line with circles: finite volume solution.

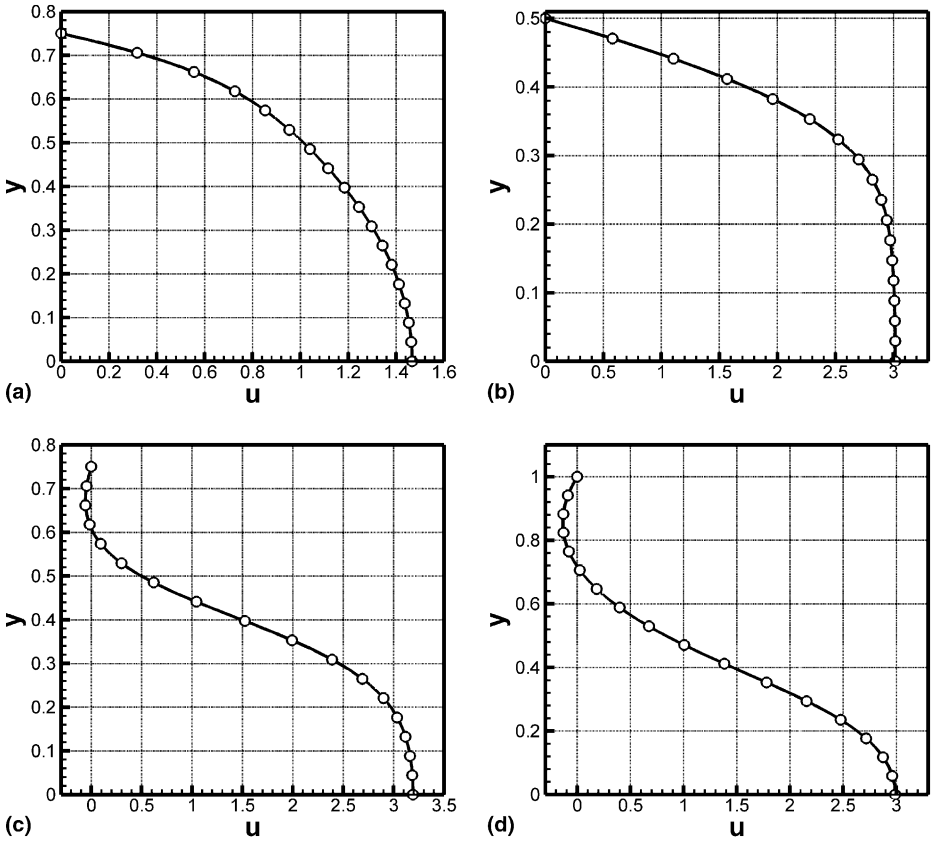

Fig. 13. Axial velocity profiles for the axisymmetric stenosed pipe simulation at (a) $x = 2.43$; (b) $x = 3.87$; (c) $x = 5.30$; (d) $x = 6.98$ Continuous line: spectral solution. Dashed line with circles: finite volume solution.

Table 5
Differences of the basic flow variables as calculated by the spectral and finite volume codes for the axisymmetric stenosed pipe flow

x_0	$D_u^{x_0}$	$D_v^{x_0}$	$D_p^{x_0}$
2.43	1.38×10^{-3}	1.41×10^{-3}	9.57×10^{-3}
3.87	5.61×10^{-3}	4.09×10^{-4}	8.64×10^{-3}
5.30	6.04×10^{-3}	5.97×10^{-4}	3.20×10^{-3}
6.98	3.30×10^{-3}	1.88×10^{-4}	2.73×10^{-3}

code, are reported in Table 5, for the specific axial positions presented in Fig. 13. Very good agreement was concluded.

With the aid of this problem, we were able to test our methodology in a spatial domain with corners in which a strong collocation method does not give adequate results, because the boundary as well as the grid is only C^0 and not C^1 continuous across elemental boundaries. Moreover, we need to say that the present method behaved satisfactorily and did not face any difficulty neither by impulsive starting nor by the form of the outflow boundary conditions. Finally, we conclude our discussion by stating that our treatment of the axis singularity by means of the modifications (15), was successful and made the weak collocation method applicable to domain decomposed topologies for axisymmetric simulations.

6. Conclusions

In this paper, we have presented a weak Legendre spectral collocation method, for the solution of the incompressible Navier–Stokes equations in two-dimensional and axisymmetric geometries. This method combines a second-order accurate temporal discretization projection method, with a weak collocation approximation for the spatial discretization of problems in decomposable topologies. The time integration method leads to a family of elliptic kernels to be solved at each time level and the spatial approximation method proceeds with discretizing these elliptic problems by using a weak formulation of the Legendre spectral collocation method in multiple subdomains. The treatment of subdomain interfaces results naturally from the discrete variational formulation of the problem. Moreover, we have furnished a weak formalism for the influence matrix technique, in order to successfully decouple the solution of the global system of discrete equations into a series of successive solutions to less expensive problems on the subdomains and on their boundaries. We also proposed a method of avoiding the singularity problem encountered by the weak formulation at axisymmetric problems and studied a combination of direct methods for solving the linear algebraic systems that stem from the spatial discretization. Several examples have been included in order to show the behavior of the method on both Stokes and Navier–Stokes simulations. Spectral accuracy was demonstrated on all problems for which exact solutions were known. For the case of problems for which no analytical solution is available, our results were proven to be in very good agreement with other methods including strong spectral collocation approximations as well as finite volume discretizations. The results of various test cases considered, indicated the robustness of the method with respect both to initial as well as to boundary conditions.

The present methodology was designed in order to overcome some difficulties faced by the strong collocation formulation when applied to multiple domains and complicated geometries. By using the weak formalism, we succeeded in approximating elliptic partial differential equations with increased accuracy, since the imposition of Neumann (or Robin) boundary conditions at the corners of the domain is being done in a natural way. The same applies to interface points at which more than two subdomains meet and to corner points that simultaneously belong to the interface and to the Neumann portion of the boundary. In such situations, the conditions imposed by a strong collocation method are totally unclear. The weak

formulation is also better than the spectral flux balance interface technique, since it is imposed pointwise and does not require any integral evaluations. Moreover, the global flux balance method does not function satisfactorily when applied to domain decomposed problems with Neumann boundary conditions. The present method is based on a modified variational formulation and as a consequence it can easily treat unstructured subdomain decomposition as well as grids or boundaries which are not C^1 continuous. The proposed combination of the influence matrix technique with the LU factorization and matrix-diagonalization methods for the solution of the linear systems was found to be very computationally efficient, while the complete decoupling of the solutions in the subdomains and on the interface (which initially results from the modified discrete variational formulation) constitutes this method as a useful alternative to existing spectral element algorithms.

Acknowledgements

The first author thanks the Greek State Scholarships Foundation for its support.

References

[1] C. Canuto, M.Y. Hussaini, A. Quarteroni, T.A. Zang, Spectral Methods in Fluid Dynamics, Springer Verlag, New York, 1987.
[2] J.P. Boyd, Chebyshev and Fourier Spectral Methods, Dover, 2001.
[3] R.D. Henderson, G.E. Karniadakis, Unstructured spectral element methods for simulation of turbulent flows, J. Comput. Phys. 122 (1995) 191.
[4] G.E. Karniadakis, Spectral element simulations of laminar and turbulent flows in complex geometries, Appl. Numer. Math. 6 (1989/90) 85.
[5] A. Pinelli, A. Vacca, A. Quarteroni, A spectral multidomain method for the numerical simulation of turbulent flows, J. Comput. Phys. 136 (1997) 546.
[6] C.L. Streett, M.Y. Hussaini, A numerical simulation of the appearance of chaos in finite length Taylor–Couette flow, Appl. Numer. Math. 7 (1991) 41.
[7] K.Z. Korczak, A.T. Patera, An isoparametric spectral element method for solution of the Navier–Stokes equations in complex geometry, J. Comput. Phys. 62 (1986) 361.
[8] A.T. Patera, A spectral element method for fluid dynamics: laminar flow in a channel expansion, J. Comput. Phys. 54 (1984) 468.
[9] D.A. Kopriva, Multidomain spectral solution of compressible viscous flows, J. Comput. Phys. 115 (1994) 184.
[10] D.A. Kopriva, J.H. Kolias, A conservative staggered-grid Chebyshev multidomain method for compressible flows, J. Comput. Phys. 125 (1996) 244.
[11] D.A. Kopriva, A staggered-grid multidomain spectral method for the compressible Navier–Stokes equations, J. Comput. Phys. 143 (1998) 125.
[12] S.A. Orszag, M. Israeli, M.O. Deville, Boundary conditions for incompressible flows, SIAM J. Sci. Comput. 1 (1986) 75.
[13] G.E. Karniadakis, M. Israeli, S.A. Orszag, High-order splitting methods for the incompressible Navier–Stokes equations, J. Comput. Phys. 97 (1991) 414.
[14] H. Le, P. Moin, An improvement of fractional step methods for the incompressible Navier–Stokes equations, J. Comput. Phys. 92 (1991) 369.
[15] A.G. Tomboulides, M. Israeli, G.E. Karniadakis, Efficient removal of boundary-divergence errors in time-splitting methods, J. Sci. Comput. 4 (1989) 291.
[16] S. Hugues, A. Randriamampianina, An improved projection scheme applied to pseudospectral methods for the incompressible Navier–Stokes equations, Int. J. Numer. Methods Fluids 28 (1998) 501.
[17] D.L. Brown, R. Cortez, M.L. Minion, Accurate projection methods for the incompressible Navier–Stokes equations, J. Comput. Phys. 168 (2001) 464.
[18] I. Rapso, S. Hugues, E. Serre, A. Randriamampianina, P. Bontoux, A spectral projection method for the simulation of complex three-dimensional rotating flows, Comput. Fluids 31 (2002) 745.
[19] C. Carlenzoli, P. Gervasio, Effective numerical algorithms for the solution of algebraic systems arising in spectral methods, Appl. Numer. Math. 10 (1992) 87.
[20] Y. Morchoisne, Inhomogeneous flow calculations by spectral methods: mono-domain and multi-domain techniques, in: R.G. Voigt, D. Gottlieb, M.Y. Hussaini (Eds.), Spectral Methods for Partial Differential Equations, SIAM-CMBS, Philadelphia, 1984, p. 181.

[21] M.G. Macaraeg, C.L. Streett, Improvements in spectral collocation discretization through a multiple domain technique, Appl. Numer. Math. 2 (1986) 95.
[22] C.L. Streett, M.G. Macaraeg, Spectral multi-domain for large-scale fluid dynamic simulations, Appl. Numer. Math. 6 (1989/90) 123.
[23] C.L. Streett, Spectral methods and their implementation to solution of aerodynamic and fluid mechanic problems, Int. J. Numer. Methods Fluids 7 (1987) 1159.
[24] D. Funaro, A variational formulation for the Chebyshev pseudospectral approximation of Neumann problems, SIAM J. Numer. Anal. 27 (1990) 695.
[25] G. Danabasoglu, S. Biringen, C.L. Streett, Application of the spectral multidomain method to the Navier–Stokes equations, J. Comput. Phys. 113 (1994) 155.
[26] C. Sabbah, R. Pasquetti, A divergence-free multidomain spectral solver of the Navier–Stokes equations in geometries of high aspect ratio, J. Comp. Phys. 139 (1998) 359.
[27] E. Serre, J.P. Pulicani, A three-dimensional pseudospectral method for rotating flows in a cylinder, Comput. Fluids 30 (2001) 491.
[28] J.P. Boyd, N. Flyer, Compatibility conditions for time-dependent partial differential equations and the rate of convergence of Chebyshev and Fourier spectral methods, Comput. Methods Appl. Mech. Engin. 175 (1999) 281.
[29] A.G. Tomboulides, S.A. Orszag, Numerical investigation of transitional and weak turbulent flow past a sphere, J. Fluid Mech. 416 (2000) 45.
[30] G.A. Blaisdell, E.T. Spyropoulos, J.H. Qin, The effect of the formulation of nonlinear terms on aliasing errors in spectral methods, Appl. Numer. Math. 21 (1996) 207.
[31] T.A. Zang, On the rotation and skew-symmetric forms for incompressible flow simulations, Appl. Numer. Math. 7 (1991) 27.
[32] C.R. Schneidesch, M.O. Deville, Chebyshev collocation method and multi-domain decomposition for Navier–Stokes equations in complex curved geometries, J. Comput. Phys. 106 (1993) 234.
[33] S.J. Sherwin, G.E. Karniadakis, A triangular spectral element method; applications to the incompressible Navier–Stokes equations, Comp. Meth. Appl. Mech. Eng. 123 (1995) 189.
[34] R.D. Henderson, Adaptive spectral element methods for turbulence and transition, in: T.J. Barth, H. Deconink (Eds.), High-Order Methods for Computational Physics, Springer Verlag, 1999, p. 225.
[35] O. Botella, On the solution of the Navier–Stokes equations using Chebyshev projection schemes with third-order accuracy in time, Comput. Fluids 26 (1997) 107.
[36] S. Tsangaris, T. Pappou, Finite difference and finite volume techniques for the solution of Navier–Stokes equations in cardiovascular fluid mechanics, in: G. Petrizzetti, K. Perktold (Eds.), Cardiovascular Fluid Mechanics, Springer-Verlag, Vienna, 2003.